Multipurpose peptides: the venoms of Amazonian stinging ants contain anthelmintic ponericins with diverse predatory and defensive activities

Samantha A. Nixon[1,2,10], Samuel D. Robinson[1], Akello J. Agwa[1,3], Andrew A. Walker[1,10], Shivani Choudhary[4], Axel Touchard[5], Eivind A. B. Undheim[6,7], Alan Robertson[4], Irina Vetter[1,8], Christina I. Schroeder[1,3], Andrew C. Kotze[2], Volker Herzig[1,9] and Glenn F. King[1,10]*

[1] Institute for Molecular Bioscience, The University of Queensland, St Lucia, QLD 4072, Australia

[2] CSIRO Agriculture and Food, St Lucia, QLD 4072, Australia

[3] National Cancer Institute, National Institutes of Health, Frederick, MD, 21702, USA

[4] Department of Biomedical Science, College of Veterinary Medicine, Iowa State University, Ames IA, 50011, USA

[5] CNRS, UMR EcoFoG, AgroParisTech, Cirad, INRAE, Université des Antilles, Université de Guyane, 97310, Kourou, France

[6] Centre for Biodiversity Dynamics, Department of Biology, NTNU, N-7491, Trondheim, Norway

[7] Centre for Ecological and Evolutionary Synthesis, Department of Biosciences, University of Oslo, 0316, Oslo, Norway

[8] School of Pharmacy, The University of Queensland, Woolloongabba, QLD 4102, Australia

[9] Genecology Research Centre & School of Science & Engineering, University of the Sunshine Coast, Sippy Downs, QLD 4556, Australia

[10] Australian Research Council Centre of Excellence for Innovations in Peptide and Protein Science, The University of Queensland, St Lucia, QLD 4072, Australia

***** Correspondence: Prof Glenn F. King, Institute for Molecular Bioscience, The University of Queensland, St Lucia, QLD 4072, Australia. Email: glenn.king@imb.uq.edu.au; Tel.: +61 7 3346 2025.

Category: Antibiotics and chemotherapeutics

Abstract

In the face of increasing drug resistance, the development of new anthelmintics is critical for controlling nematodes that parasitise livestock. Although hymenopteran venom toxins have attracted attention for applications in agriculture and medicine, few studies have explored their potential as anthelmintics. Here we assessed hymenopteran venoms as a possible source of new anthelmintic compounds by screening a panel of ten hymenopteran venoms against *Haemonchus contortus*, a major pathogenic nematode of ruminants. Using bioassay-guided fractionation coupled with liquid chromatography-tandem mass spectrometry, we identified four novel anthelmintic peptides (ponericins) from the venom of the neotropical ant *Neoponera commutata* and the previously described ponericin M-PONTX-Na1b from *Neoponera apicalis* venom. These peptides inhibit *H. contortus* development with IC_{50} values of 2.8-5.6 μM. Circular dichroism spectropolarimetry indicated that the ponericins are unstructured in aqueous solution but adopt α-helical conformations in lipid mimetic environments. We show that the ponericins induce non-specific membrane perturbation, which confers broad-spectrum antimicrobial, insecticidal, cytotoxic, hemolytic, and algogenic activities, with activity across all assays typically correlated. We also show for the first time that ponericins induce spontaneous pain behaviour when injected in mice. We propose that the broad-spectrum activity of the ponericins enables them to play both a predatory and defensive role in neoponeran ants, consistent with their high abundance in venom. This study reveals a broader functionality for ponericins than previously assumed, and highlights both the opportunities and challenges in pursuing ant venom peptides as potential therapeutics.

Keywords

ant; venom peptide; ponericin; antimicrobial; anthelmintic; pain

1 Introduction

Hymenopterans are a highly diverse order of insects, with more than 153,000 extant species [1]. Among these are approximately 9,000 species of stinging ants (family Formicidae) [2]. Ant venoms are chemically diverse, containing a range of peptide and small molecule toxins [3]. These toxins are employed for predation, chemical detoxification, competitor deterrence and defense, including against large animals and microbial pathogens [4-7]. The diversity of biological activities associated with ant toxins has led to increasing interest in their potential application in medicine and agriculture [8]. For example, numerous antimicrobial peptides (AMPs) have been reported in hymenopteran venoms, such as bicarinalin from the ant *Tetramorium bicarinatum* [9] and pilosulin from the ant *Myrmecia pilosula* [10], which have broad-spectrum activity against Gram-positive and Gram-negative bacteria and fungal pathogens. However, the broader anti-infective properties of these AMPs are understudied. Some hymenopteran venom-derived AMPs have antiparasitic activity, such as mastoparan from the vespid wasp *Polybia paulista*, and the dinoponeratoxins from the giant predatory ant *Dinoponera quadriceps*, which both have antitrypanosomal activity *in vitro* [11, 12]. We recently reported that the peptide Δ-myrtoxin-Mp1a from the venom of the Australian jack jumper ant *Myrmecia pilosula* has low micromolar anthelmintic activity against the pathogenic blood-feeding nematode *Haemonchus contortus* [13]. *H. contortus* serves as model for anthelmintic drug discovery, which is an urgent priority for livestock production in the face of rising drug resistance [14-16]. Parasitic helminths cost the European ruminant industry €1.8 billion annually [17], and gastrointestinal nematodes alone cost the Australian sheep industry over $450 million each year in production losses and treatments [18].

In this study, we screened ten crude hymenopteran venoms against *H. contortus* to search for new anthelmintic leads. Using bioassay-guided fractionation, we identified five anthelmintic venom peptides from ants in the *Neoponera* genus, which were revealed to be

ponericins. Ponericins are a large family of short, linear cationic AMPs within the aculeatoxin superfamily, originally described from *Neoponera goeldii* (formerly *Pachycondyla*) with antimicrobial, hemolytic and insecticidal activities [19]. They are categorised into three subfamilies, according to their sequence similarity and the predominant N-terminal amino acid: the 'melittin-like' W-subfamily with antimicrobial, insecticidal and hemolytic activity; the 'dermaseptin-like' L-subfamily with antimicrobial activity; and the 'cecropin-like' G-subfamily with both antimicrobial and insecticidal activity [2, 19]. Ponericins are widespread across the Ponerinae subfamily, with examples reported from the genera *Neoponera* [20] and *Dinoponera* [21, 22], and further from formicoid ants, such as *Ectatomma brunneum* [23]. The prevalence of these peptides suggests that they play important ecological functions for the ants; however, their ecological role has not been clearly established. We synthesised and characterised the five identified ponericins and a series of structural analogues to explore their structure-activity relationships with respect to their potential as therapeutic leads for anti-infectives. We show that the ponericins have a much broader range of biological activities than previously assumed, highlighting both opportunities and challenges for their development as antimicrobial and anthelmintic agents.

2 Materials and Methods

2.1 Insect and venom collection

The neotropical ants *Ectatomma tuberculatum*, *Neoponera apicalis*, *N. commutata*, *Odontomachus hastatus* and *Paraponera clavata* were collected from various localities in French Guiana. Crude venom samples were prepared by dissecting ant venom reservoirs in ultrapure water then pooling them in 10% acetonitrile (ACN) in ultrapure water. Venom samples were loaded into a 0.45 µm Costar® Spin-X tube filter (Corning Incorporated, Corning,

NY, USA) and centrifuged at 12,000 *g* for 3 min to remove tissues from the venom apparatus. Filtered venom samples were then lyophilised prior to storage at −20 °C until further use.

Myrmecia nigrocincta worker ants were collected near Brisbane, Australia. Venom was acquired by inciting ants to sting a thin layer of parafilm, as described previously [24]. Venom droplets were collected in 10 µL H_2O and dried by vacuum centrifugation. *M. rufinodis*, *Vespa simillima*, and *Synoeca septentrionalis* venoms collected by dissection of venom reservoirs were donated by Dr Kate Baumann and Professor Bryan Fry at The University of Queensland (UQ), Australia. Lyophilised whole *V. crabro* venom was purchased from Latoxan (Portes lés Valence, France).

2.2 Chemicals

All chemicals used in this study were purchased from Sigma-Aldrich (North Ryde, NSW, Australia) unless otherwise stated.

2.3 *Haemonchus contortus* larval development assay

Sheep were infected with *H. contortus* Kirby isolate (originally recovered from the University of New England Kirby Research Farm in 1986; susceptible to all commercial anthelmintics [25]) and housed at the Commonwealth Scientific and Industrial Research Organisation (CSIRO) FD McMaster Laboratory, Armidale, NSW, Australia. All animal procedures were approved by the FD McMaster Animal Ethics Committee (Approval Number AEC 17/12 and 18/09). Eggs were prepared from overnight fecal collection as described previously [26]. In brief, feces were filtered through mesh filters, settled, and supernatant removed by vacuum. Eggs were recovered by density centrifugation using 10 and 25% (*w*/*v*) sucrose solutions, centrifuged at 650 *g* for 7 min. Eggs were recovered from the interface of the two sucrose layers, rinsed with distilled water, sterilised with bleach, rinsed again, and

diluted to 4,500 eggs mL^{-1}. Tylosin tartrate (800 µg mL^{-1}) and amphotericin B (25 µg mL^{-1}) were added, and eggs were used immediately for larval development assays (LDAs).

Assays were conducted using 96-well microtitre plates, with each well containing 50 µL of 2% agar, 20 µL of egg solution and 20 µL of peptide solution in water as described [27]. The commercial anthelmintic levamisole (Sigma Aldrich) was used as a positive control. Negative controls contained equivalent volumes of water or DMSO (final 1% *v*/*v*). Plates were incubated at 26 °C for six days. After 24 h, each well was fed with 10 µL of a nutrient solution containing *Escherichia coli* XL1-Blue1 (grown overnight at 37 °C) and growth medium. The growth medium consisted of yeast extract (1% *w*/*v*), Earle's salt solution (10% *v*/*v*), saline solution (0.9% NaCl, *w*/*v*), and sodium bicarbonate (1 mM) in Luria-Bertani medium (LB). Larvae were killed and stained with Lugol's iodine solution after six days. Larvae that had developed to the infective L3 stage were counted, and the numbers in treated assay wells were expressed as a percentage of the number of infective L3 stage larvae in multiple control wells. Concentrations that caused 50% inhibition (IC_{50} values) were calculated from three experiments of triplicate assays via non-linear regression using Prism 8.0 (GraphPad Software, San Diego, CA, USA), and statistical differences between peptides were calculated using one-way ANOVA with Tukey's post-hoc correction.

2.4 Bioactive peptide isolation

N. apicalis (400 µg) and *N. commutata* venom (500 µg) were fractionated via reversed-phase high-performance liquid chromatography (RP-HPLC) using a Gemini NX-C_{18} column (250 × 4.6 mm; particle size 3 µM, pore size 110 Å; Phenomenex, Torrance, CA, USA) with a 5 to 80% gradient of solvent B (90% ACN and 0.05% trifluoroacetic acid (TFA)) in solvent A (0.05% TFA in water) over 50 min at a flow rate of 1 mL min^{-1}. Fractions were collected on the basis of absorbance at 214 nm, lyophilised and tested against *H. contortus* in a LDA. Active

fractions were further purified using either an Phenomenex Onyx C_{18} monolithic column (100 × 3.0 mm, pore size 130 Å) with a gradient of 5 to 60% solvent B over 40 min at flow rate 1 mL min^{-1}, or a VisionHT HILIC column (150 × 4.6 mm, pore size 5 µM; Grace, Epping, VIC, Australia) with a gradient of 95 to 5% solvent B over 30 min at flow rate 1 mL min^{-1}, and then re-tested against *H. contortus.*

2.5 Proteotranscriptomic identification of peptide amino acid sequences

Peptide monoisotopic masses were determined using matrix-assisted laser desorption-time of flight mass spectrometry (MALDI-TOF MS), where 0.4 µL of reconstituted HPLC fraction was spotted together with 0.4 µL α-cyanohydroxycinnamic acid (CHCA) dissolved at 7.5 mg mL^{-1} in 70% ACN with 0.05% TFA with 10 min sonication. After drying, samples were analysed using a SCIEX TOF/TOF 5800 MALDI mass spectrometer operated in reflectron-positive mode, with laser power 3,000–5,000 and acquisition range 500–4,500 *m/z*. An anthelmintic fraction from *N. apicalis* venom was further analysed using the matrix 1,5-diaminonapthalene (1,5-DAN, prepared and analysed as above) and subsequent peptide fragmentation was compared against a database of known *Neoponera* peptides [2].

To delineate venom-peptide sequences, we combined transcriptomics and proteomics. For transcriptomics, total RNA was extracted from a pool of 12 *N. commutata* venom apparatus (venom reservoir plus venom glands) dissected from live worker ants. The venom-gland tissues were disrupted with a TissueLyser II (Qiagen, Germantown, MD, USA) in RLT buffer containing 10% (v/v) of 2-mercaptoethanol (Rneasy Mini Kit, Qiagen). RNA was first isolated with a phenol-chloroform (5:1) solution followed by washing with a solution of chloroform-isoamyl alcohol (25:1) to remove phenol. The RNA was then bound to a Qiagen column and washed as per the manufacturer's instructions. DNAse I (Roche Diagnostics GmbH, Mannheim, Germany) was added to remove DNA fragments. The RNA was eluted in 50 µL

of RNase-free water and a NanoDrop 2000c UV-Vis spectrophotometer (Thermo Fisher Scientific, Wilmington, DE, USA) was used to determine 260/280 and 260/230 nm ratios. Finally, RNAstable® LD (Biomatrica, San Diego, CA, USA) was added to the purified RNA and the sample was dried using a Speed Vac (RC1010, Jouan, Saint Herblain, France). Dried RNA samples were shipped to the UQ Institute for Molecular Bioscience (IMB), then TruSeq library preparation and sequencing on an Illumina MiSeq sequencer (San Diego, CA, USA) was performed by the IMB Sequencing Facility. 42,137,392 2 × 150 bp paired-end reads were generated, which were trimmed using Trimmomatic 2.2.0 default parameters and assembled using Trinity 2.2.0 with minimum contig size 150 bp. From the resulting transcriptome of 34,187 contigs, a database of 45,818 possible amino acid sequences was extracted using TransDecoder 5.3.0 with minimum open reading frame size 90 bp. This amino acid sequence database, together with a list of common contaminant proteins, was used as a search database to identify peptide sequences by searching mass spectral data.

To generate spectral data, purified native peptide samples without reduction, alkylation, or proteolytic digestion (~25 µg estimated using a Nanodrop 2000c spectrophotometer; Thermo Scientific, Waltham, MA, USA) were analysed via LC-MS/MS using a SCIEX 5600 triple-TOF mass spectrometer (Framingham, MA, USA) equipped with a Turbo V ion source and coupled to a Nexera X2 LC system (Shimadzu, Kyoto, Japan). Peptides were separated using a Zorbax 300SB-C_{18} column (2.1 × 100 mm, particle size 5 µM, pore size 300 Å; Agilent, Santa Clara, CA, USA) incubated at 60 °C. Peptides were eluted over 14 min using a gradient of 1 to 40% LCMS solvent B (90% ACN/ 0.1% formic acid (FA)) in solvent A (0.1% FA) at a flow rate of 0.2 mL min^{-1}. MS^1 scans were collected between 350 and 2,200 *m/z*, and precursor ions in the range *m*/*z* 350–1,500 with a charge from +2 to +5 and signal >100 counts/s were selected for analysis, excluding isotopes within 2 Da. MS/MS scans were acquired with an accumulation time of 250 ms and cycle time of 4 s. The 'Rolling collision energy' option was

selected in Analyst software, allowing collision energy to be varied dynamically based on *m*/*z* and *z* of the precursor ion. Up to 20 similar MS/MS spectra over *m*/*z* range 80–1,500 were pooled from precursor ions differing by <0.1 Da. The resulting MS and MS/MS data were then compared against a draft venom gland transcriptome database using the Paragon and Protgroup algorithms in ProteinPilot 4.5 software (SCIEX, Framingham, MA, USA).

2.6 Solid phase peptide synthesis

A Symphony automated peptide synthesiser (Gyros Protein Technologies, Tucson, AZ, USA) was used for assembly of the peptides using a 2-chlorotrityl chloride resin, substitution value 0.8 mmol/g, on a scale of 0.125 mmol using standard Fmoc chemistry as previously described [28-30]. Cleavage of protecting groups was achieved over 2 h at room temperature with simultaneous release from the resin using a cocktail containing 96% (*v/v*) TFA, 2% (*v/v*) water and 2% (*v/v*) triisopropylsilane [28]. TFA was removed using a rotor vaporiser and ice-cold diethyl ether was used to precipitate the peptides. After filtration to remove cleavage waste, the peptides were solubilised in 45% (*v/v*) ACN and 0.05% (*v/v*) TFA, then lyophilised.

Crude peptides were purified using RP-HPLC with a gradient of 10–60% HPLC solvent B (90% *v/v* ACN; 0.05% *v/v* TFA) in HPLC solvent A (0.05% TFA) over 50 min at a flow rate of 50 mL min^{-1} (Phenomenex Jupiter C_{18} column, 250 × 50 mm, particle size 10 μm; Phenomenex, Torrance, CA, USA). Semi-pure peptides were then purified further using a gradient of 10–60% solvent B over 70 min at a flow rate of 8 mL min^{-1} using an Agilent C_{18} column (250 × 30 mm, particle size 5 μM, pore size 100 Å; Agilent technologies, CA), and then using a linear gradient of 20–50 % solvent B over 60 min at a flow rate of 3 mL min^{-1} with a Phenomenex Gemini C_{18} column (250 × 10 mm, particle size 5μm, pore size 110 Å). Fractions were collected and analysed using ESI-MS. Purity of fractions was confirmed to be >95% based on area under the HPLC peak when analysed on an analytical C_{18} column

(Grace Vydac 150 × 2.1 mm, particle size 5 μm, pore size 120 Å; Thermo Fisher Scientific, Waltham, MA, USA) using a flow rate of 0.3 mL min^{-1} and a gradient of 0–60% HPLC solvent B over 30 min. Pure fractions were pooled, lyophilised and stored at –20 °C [28-30]. Synthetic toxins were co-eluted with their native counterpart on a Phenomenex Kinetex C_{18} analytical column (250 × 4.6 mm, particle size 5 μM, pore size 100 Å) using a gradient of 5–60% solvent B over 60 min with a flow rate of 1 mL min^{-1}.

2.7 *Brugia malayi* adult motility assay

B. malayi male adult worms were provided by the NIH/NIAID Filariasis Research Reagent Resource Center (FR3; College of Veterinary Medicine, University of Georgia, Athens, GA, USA), and the protocols for worm handling were approved by the Institutional Biosafety Committee (IBC) at Iowa State University. We maintained the adult worms in 24-well culture plates (1 worm/well) containing 2 mL of non-phenol red Roswell Park Memorial Institute (RPMI) 1640 media (Life Technologies, USA) supplemented with 10% heat-inactivated fetal bovine serum (FBS, Fisher Scientific, USA) and 1% penicillin-streptomycin (Life Technologies, USA) and stored at 37 °C supplemented with 5% CO_2. The Worminator system was used to study the effect of *Neoponera* venom peptides on worm motility in a 24-well microtiter plate [31, 32]. The WormAssay v1.4 software measures each worm's pixel displacement over time with Mean Movement Unit (MMU) as output. Each worm was placed in a single well of the microtiter plate containing 1 mL of supplemented RPMI media. Stock solutions (0.3–30 mM) of the ant peptides were prepared in distilled water, and 1 μL of the stock solution was added to each well to obtain the final concentrations (0.3–30 μM). Once the peptides were added, worm motility was recorded at 0, 1, 2, 4, 6, 24, 48, 72, and 96 h post-treatment. The anthelmintic drug emodepside (10 μM) was used as a positive control, and 1 μL distilled water was used as a negative control. We calculated the % motility as a percentage

ratio of motility of worms after treatment at each time point over motility of naïve worms using four worms per peptide per experiment, with three technical repeats.

2.8 Insecticidal activity against sheep blowflies

The insecticidal activity of synthetic ponericins was monitored using a previously described blowfly assay [33, 34]. In brief, peptides were dissolved in water and 2 µL was injected into the thorax of adult sheep blowflies (*Lucilia cuprina*, within 24–48 h of emerging, mass 22.0–31.5 mg). Flies were housed individually in 2 mL tubes and paralytic activity and lethality determined at 0.5, 1 and 24 h post-injection. Each toxin was tested at 4–6 doses (n = 10 flies per dose) with corresponding water controls (n = 30 per peptide), with three technical replicates per peptide. Toxin effects were normalised against controls using the Henderson-Tilton equation and median paralytic (PD_{50}) and lethal (LD_{50}) doses calculated in Prism 8.0 as described [33]. Statistical differences were calculated using one-way ANOVA with Tukey's post-hoc correction in GraphPad Prism v9.0 (San Diego, CA, USA).

2.9 Antimicrobial assay

Synthetic ponericins were serially diluted two-fold in cation-adjusted Mueller Hinton Broth (CaMHB; Bacto Laboratories, Mt Pritchard, NSW, Australia) and plated in duplicate on non-binding surface 96-well plates (Corning). Bacteria (strains listed in Table 2) were cultured in CaMHB medium at 37 °C overnight, then diluted 40-fold and incubated at 37 °C for a further 2–3 h. The resultant mid-log phase cultures were diluted in CaMHB medium and added to each well to give a final cell density of 5×10^5 CFU mL^{-1}, and a final compound concentration range of 0.06–128 µg mL^{-1}. Plates were covered and incubated at 37 °C for 20 h. Inhibition of bacterial growth was determined visually, where the minimum inhibitory concentration (MIC) was recorded as the lowest compound concentration that yielded no visible growth.

2.10 Cytotoxicity assay

HEK293 cells (ATCC® CRL-1573) were seeded at 3,000 cells/well in 20 μL DMEM medium (GIBCO-Invitrogen, Grand Island, NY, USA) with 10% FBS (Scientifix, Clayton, Vic, Australia) in clear bottom 384-well plates. Cells were incubated at 37 °C in 5% CO_2 for 24 h to allow cell attachment. Compounds were dissolved in water at 1.28 mg mL^{-1} with subsequent three-fold dilutions in cell culture medium, giving a final concentration range of 0.02–50 μg mL^{-1}. Tamoxifen (Sigma-Aldrich,) was used as a negative cell both at a single concentration (100 μM) and using multiple concentrations (0.18 to 400 μM) to give a concentration-response curve. Cells were incubated with compounds for 24 h at 37 °C, 5% CO_2. After incubation, 10 μM resazurin (Sigma-Aldrich, dissolved in PBS) was added to each well and the plates were incubated for a further 3 h at 37 °C, 5% CO_2. Fluorescence intensity was measured using a Polarstar Omega spectrophotometer (BMG Labtech, Mornington, Australia) with excitation/emission of 560/590 nm. The concentration required to induce 50% cell death (CC_{50}, determined as 50% reduction in absorbance relative to untreated control) was calculated using Prism 8.0. Cytotoxicity assays were performed as two independent experiments of duplicate assays to obtain data of $n = 2$.

2.11 Hemolysis assay

Whole human blood (10 mL per tube) was washed in triplicate with three volumes of 0.9% w/v NaCl, with centrifugation at 500 *g* (with reduced deceleration) for 10 min between washes. Cells were counted with a hemocytometer and then diluted to 0.5×10^8 mL^{-1} in 0.9% NaCl. Cell suspension (180 μL/well) was added to assay plates and then plates were sealed and incubated at 37 °C for 1 h. Plates were then centrifuged at 1000 *g* for 10 min to pellet cells and debris, then 25 μL of supernatant was recovered into a 384-well flat bottom polystyrene plate. Absorbance was read at 405 nm using a Tecan M1000 Pro monochromator plate reader. The

percentage hemolysis was calculated for each well relative to the negative control (1% DMSO in PBS) and positive control (1% Triton X-100 in PBS). Significant differences in hemolysis values were determined by fractional deviation from the mean, calculated using the average and standard deviation of the sample wells (no controls) on the same plate. The concentration required to lyse 50% of the red blood cells (HC_{50}) was determined from two independent experiments of duplicate assays to obtain data of $n = 2$.

2.12 Calcium imaging of mammalian sensory neurons

Calcium imaging of mouse dorsal root ganglion (DRG) sensory cells was performed as previously described [24]. In brief, DRG cells isolated from 4–8-week-old male C57BL/6 mice (under The University of Queensland Animal Ethics Committee approval TRI/IMB/093/17) were dissociated and plated in Dulbecco's modified Eagle's medium (ThermoFisher Scientific, Grand Island, NY, USA) containing 10% FBS (Assaymatrix, Melbourne, Australia) and penicillin/streptomycin (ThermoFisher) on a 96-well poly-D-lysine–coated culture plate (Corning), and maintained overnight. Cells were loaded with Fluo-4 AM calcium indicator as per the manufacturer's instructions (ThermoFisher). After loading for 1 h, the dye solution was replaced with assay solution (Hanks' balanced salt solution and 20 mM HEPES). Fluorescence corresponding to intracellular calcium ($[Ca^{2+}]_i$) of typically 100–150 DRG cells per experiment was monitored in parallel using a Nikon Ti-E deconvolution inverted microscope, equipped with a Lumencor Spectra LED light source. Images were acquired at a 20× objective at one frame/s (excitation 485 nm; emission 521 nm). For each experiment, baseline fluorescence was monitored for 30 s and then a wash of assay solution was applied. At 60 s, the assay solution was replaced with assay solution containing individual peptides (10 μM) and the cells were observed for a further 90 s.

2.13 FLIPR assay

F11 and HEK293 cells were cultured as previously described [24]. Cells were maintained in Ham's F12 media supplemented with 10% FBS, 100 µM hypoxanthine, 0.4 µM aminopterin, and 16 µM thymidine (Hybri-MaxTM, Sigma Aldrich, North Ryde, Australia). 384-well imaging plates (Corning) were then seeded 48 h prior to imaging, which yielded 90–95% confluence at the time of imaging. Cells were incubated for 30 min with the Calcium 4 assay component A according to the manufacturer's instructions (Molecular Devices, Sunnyvale, CA, USA) in physiological salt solution (PSS; composition in mM: 140 NaCl, 11.5 D-glucose, 5.9 KCl, 1.4 $MgCl_2$, 1.2 NaH_2PO_4, 5 $NaHCO_3$, 1.8 $CaCl_2$, 10 HEPES) at 37 °C. Fluorescence was measured using a fluorescent plate reader ($FLIPR^{TETRA}$) equipped with a CCD camera (Excitation: 470–490 nm, Emission: 515–575 nM) (Molecular Devices, Sunnyvale, CA, USA). Signals were read every second for 10 s before, and 300 s after the addition of peptides in PSS supplemented with 0.1% bovine serum albumin (BSA). All data are mean ± SEM of assays performed in triplicate. Maximum–minimum fluorescence in the 300 s period after peptide addition was recorded as the response. Concentration-response data were fitted with a four-parameter Hill equation (variable slope) using Prism 8.0 to obtain effective concentration (EC_{50}) values.

2.14 *In vivo* nocifensive responses

C57BL/6J mice (male adults, 4 weeks old) were used for behavioural experiments. Synthetic ponericins (600 pmol) diluted in sterile saline containing 0.1% BSA were administered in a volume of 20 µL into the right hindpaw by shallow (subdermal) intraplantar injection. Control animals were injected with vehicle (sterile saline containing 0.1% BSA). Spontaneous pain behaviour was counted from video recordings by a blinded observer. Experiments were approved by UQ Animal Ethics Committee (Approval PHARM/526/18).

2.15 Secondary structure determination using circular dichroism spectropolarimetry

The secondary structure of synthetic ponericin peptides was evaluated via circular dichroism (CD) on a JASCO-810 spectropolarimeter (JASCO, Eaton, MD, USA) operated at 25 ºC. The wavelength range 185–260 nm was scanned at 50 nm min^{-1}. CD spectra were obtained as the average of five scans, from which the solvent spectrum was subtracted and Gaussian smoothing applied. Peptides (25 µM) were analysed in water, 20 mM sodium dodecyl sulfate (SDS) and 2,2,2-trifluoroethanol (TFE) at 20% v/v. α-Helical wheel projections were generated using the online tool NetWheels (lbqp.unb.br/NetWheels/) [35].

3 Results

3.1 Identification of anthelmintic novel ponericins

We screened ten hymenopteran venoms (seven ant and three wasp species) against *H. contortus* in a LDA. All venoms inhibited larval development by > 50% at 0.2 mg mL^{-1} (Fig. 1). The most potent venoms were those from the Amazonian stinging ants *N. apicalis* and *N. commutata*, which yielded complete inhibition at 0.2 mg mL^{-1} and >50% inhibition at 0.05 mg mL^{-1}, with clear larval death immediately post-hatching (Fig. 1). We used bioassay-guided fractionation with successive HPLC steps to identify four active fractions from *N. commutata* venom, which corresponded to the four largest peaks in the RP-HPLC chromatogram of whole venom, and one active fraction from *N. apicalis* venom (Fig. 2). MALDI-TOF analysis indicated that the active fractions contained peptides with masses in the range 2.4–3.4 kDa (Table 1).

To identify the primary structure of the anthelmintic peptides from *N. commutata* venom, we used a combined transcriptomic/proteomic approach. LC-MS/MS data derived from native peptides (without reduction, alkylation, or proteolytic digestion) were used to

search an amino acid database of translated open reading frames extracted from a venom-gland transcriptome using ProteinPilot software. This process yielded high confidence identifications (>99%) for each of the four isolated peptides. In each case, we observed that the theoretical monoisotopic mass of the identified amino acid sequence closely matched the observed monoisotopic mass (Table 1), suggesting that the identified sequences were correct and free of post-translational modifications. The four novel *N. commutata* peptides were named M-PONTX-Nc1a (hereafter Nc1a), Nc1b, Nc1c and Nc1d based on the rational nomenclature for venom peptides [3] (listed in Table 1).). For the anthelmintic peptide isolated from *N. apicalis* venom, we collected MALDI-TOF spectra in the presence of the matrix 1,5-DAN, which induces in-source decay fragmentation. This yielded a sequence of eight residues which matched the C-terminal region of M-PONTX-Na1b (hereafter Nalb) previously identified from the same ant species [2, 3]. Subsequent LCMS/MS product ion spectra were used to confirm the full sequence as Na1b, which matched the observed monoisotopic mass. Notably, all of the five anthelmintic peptides are short linear peptides that are rich in lysine (13–20%) and have a net positive charge at physiological pH.

A BLAST search of the NCBI non-redundant protein database revealed that the five anthelmintic peptides have high sequence similarity (E values < $1e^{-05}$) to previously described ponericins from *N. goeldi* and *N. inversa* [2, 19]. Na1b and Nc1a are most similar to the 'melittin-like' W-subfamily (88% and 60% similarity respectively), Nc2a to the 'dermaseptin-like' L-subfamily (60% similarity), and Nc3a and Nc3b to the 'cecropin-like' G-subfamily (73% and 68% similarity respectively). Toxin sequence alignments to the respective ponericins are shown in Figure 3.

3.2 Bioactivity of synthetic ponericins

Ponericins have previously been shown to have insecticidal, antimicrobial and hemolytic activity [2, 19], but the relationship between their ecological functions and potential biomedical applications is poorly understood. To further examine the biological activities of anthelmintic ponericins, we synthesised each peptide using Fmoc solid-phase peptide synthesis and purified them to >95% homogeneity (Fig. 4). The synthetic ponericins matched their native counterparts in mass (Fig. 4), and co-eluted with them on RP-HPLC. The synthetic peptides were thus presumed to be identical to the venom-derived peptides and were used to investigate their bioactivity in the remainder of the study.

3.2.1 Ponericins show potent anthelmintic activity against H. contortus in vitro

To confirm the anthelmintic activity of the isolated ponericins and obtain precise IC_{50} values using the greater quantity of peptide available, we repeated the *H. contortus* LDA using synthetic peptides. Na1b, Nc1a and Nc3a potently inhibited larval development with IC_{50} values <6 µM, as shown in Fig. 5A and summarised in Table 3. The ponericins had a concentration-dependent effect on larval development, with larvae dying immediately after hatching at high concentrations (>30 µM) whereas larval motility was impaired, and development delayed, at lower concentrations (1–20 µM). Visual inspection confirmed *E. coli* growth in affected wells, indicating that the ponericins exerted a direct anthelmintic effect rather than indirectly killing larvae through starvation due to antimicrobial activity. Na1b had the strongest anthelmintic activity, with an IC_{50} (2.8 ± 0.3 µM) that is only four-fold higher than the commercial anthelmintic levamisole (IC_{50} 0.71 ± 0.1 µM). Nc2a and Nc3b have moderate anthelmintic activity (IC_{50} 23–38 µM). Despite their sequence similarity (77%), one-way ANOVA indicated that Nc3a was significantly more potent against *H. contortus* than Nc3b ($p < 0.05$).

The potent anthelmintic activity of these ponericins against *H. contortus* prompted us to screen the peptides against the important human filarial parasite *Brugia malayi* to determine if the anthelmintic activity extended to other pathogenic nematodes. At a concentration of 10 µM, Nc3a and Nc3b significantly reduced the motility of adult male *B. malayi*, whereas 10 µM Nc2a and 30 µM Nc1b failed to exhibit any significant inhibitory effects. Interestingly, treatment with Nc1a increased worm motility for 24 h post-treatment, followed by a reduction in motility for the rest of the experiment. This hypermotility effect was only significant at 10 µM concentration (Fig. 5B).

3.2.2 Ponericins induce paralysis in blowflies

The anthelmintic activity of the isolated ponericins seems unlikely to be their natural function. Since *Neoponera* ants use their venom to subdue prey, typically small arthropods [7], we assessed the insecticidal activity of ponericins using sheep blowflies (*L. cuprina*) as a model insect. Injection of the ponericins resulted in rapid contractile paralysis that persisted for several hours, which for Nc1a and Nc3a progressed to lethality by 24 h (Fig. 5C–D). Nc3a was the most active peptide, with a PD_{50} of 0.50 ± 0.03 nmol g^{-1} and LD_{50} of 3.50 ± 0.03 nmol g^{-1}. In contrast, Na1b, Nc2a and Nc3a induced reversible paralysis, with PD_{50} values of 25.8–31.4 nmol g^{-1}, but high doses failed to kill flies (LD_{50} >100 nmol g^{-1}).

3.2.3 Ponericins activate sensory neurons and induce spontaneous pain

Neoponera ants also use their venom defensively, and stings are reported to cause pain [6]. We therefore investigated the algogenic activity of the ponericins by examining their ability to stimulate mouse DRG sensory neurons *in vitro.* Addition of 10 µM Na1b, Nc1a and Nc3a caused an immediate rapid increase in intracellular calcium concentration ($[Ca^{2+}]_i$) in all DRG cells, including neuronal and non-neuronal cells (Na1b and Nc1a shown in Fig. 6A,D).

Over the time course of the experiment, most cells showed a subsequent decrease in $[Ca^{2+}]_i$, with a corresponding increase in fluorescence in the extracellular medium (Fig. 6B,E), indicating leakage of the calcium-sensitive dye from the cells through pore formation or lysis. This was most prominent for Nc3a, which induced rapid and near total cell lysis (Fig. 6D, E). In contrast, Nc2a and Nc3b did not induce an increase in $[Ca^{2+}]_i$ at 10 µM (not shown).

The potency of each peptide was quantified via a high-throughput $[Ca^{2+}]_i$ assay using F11 cells (a neuroblastoma/DRG neuron hybrid cell line). Consistent with the dye leakage observed in the DRG assay, Na1b, Nc1a and Nc3a induced an initial increase in fluorescence, followed by a decrease consistent with quenching of the fluorescent Ca^{2+} dye following membrane disruption. Na1b and Nc1a showed the most potent effect (EC_{50} 0.9–1.5 µM), Nc1a and Nc3a showed moderate activity (EC_{50} 22–40 µM), and Nc3b was completely inactive (EC_{50} >100 µM, Fig. 6F–M). We repeated this experiment in non-excitable HEK293 cells to probe whether this effect was driven by ion channel modulation or membrane-perturbation (Fig. 6C). We found that ponericins exerted similar effects on neuronal (F11) and epithelial (HEK293) cell lines, with Na1b and Nc1a showing significantly more potent activity across both cell lines than the other ponericins ($p < 0.05$ by one-way ANOVA). Na1b and Nc1a were equipotent in F11 and HEK293 cells, supporting a non-specific membrane perturbation mechanism of action, rather than activity on a sensory neuron-specific ion channel.

We then assessed the algogenic effects of Na1b, Nc1a and Nc3a *in vivo* by intraplantar injection of peptide into the hindpaw of C57BL/6 mice. Consistent with the observed effects *in vitro*, the synthetic ponericins induced spontaneous nocifensive behaviour *in vivo* (licking, biting, scratching and shaking of the injected paw). Na1b induced the strongest response, peaking around 15 min post-injection and then decreasing over 30 min ($p < 0.05$, Fig. 6N). Nc1a peaked at 5 min post-injection (Fig. 6O). Nc3a induced a moderate response, similarly

peaking early at 5 min post-injection and then rapidly decreasing (Fig. 6P). These data suggest that the ponericins likely serve a defensive function by inducing pain in vertebrate predators.

3.2.4 Antimicrobial activity

Given the membrane-disrupting mode of action of ponericins, we hypothesised they may also have antibacterial activity, similar to other venom-derived cationic peptides including pilosulins and ponericins from related ant venoms [19, 36]. Hence, we submitted the synthetic ponericins to the Community for Open Antimicrobial Drug Discovery (CO-ADD) where they were screened against a panel of pathogenic Gram-positive and Gram-negative bacteria (Table 2). Na1b and Nc3a were found to have the strongest and most broad-spectrum antimicrobial activity, with MIC values typically less than 20 µM across both Gram-positive and negative bacteria. The pathogens *Acinetobacter baumannii* and *Bacillus subtilis* were the most susceptible microbes tested (MIC 1.4–2.9 µM). Interestingly, Nc3a was the only peptide to show activity against *Pseudomonas aeruginosa* (MIC 11.8–23.7 µM), while Nc3b appeared inactive against bacteria, with MIC >40 µM across all strains tested. Nc1a was more active against Gram-positive bacteria (*Staphylococcus aureus* and *B. subtilis*, MIC 1.48–5.9 µM) than Gram-negative bacteria. Nc2a, with greatest homology to the antibacterial L-subfamily of ponericins, showed moderate activity against *E. coli*, *A. baumannii*, and *B. subtilis.*

3.2.5 Cytotoxicity and hemolysis of mammalian cells

The data obtained above, along with the previously reported hemolytic activity of ponericins, particularly from W-subfamily [19], prompted us to test the novel synthetic ponericins for cytotoxic activity against human erythrocytes and HEK293 cells. The W-subfamily peptides Na1b and Nc1a and G-subfamily peptide Nc3a showed pronounced cytotoxic effects, with EC_{50} values less than 6 µM, approximately equal to their IC_{50} values

against *H. contortus.* Nc2a showed moderate activity (EC_{50} >40 µM) while Nc3b was inactive up to 100 µM. In general, the ponericins were less potent against red blood cells than HEK293 cells; Nc2a, Nc3a and Nc3b had EC_{50} values for hemolysis exceeding 100 µM, while Nc3b induced no hemolysis even at a concentration of 300 µM. Na1b and Nc1a had moderate hemolytic activity with EC_{50} values of 28–60 µM. Cytotoxicity and hemolysis values are summarised in Table 3.

3.2.6 Ponericins adopt α-helical conformations in lipid environments

The results outlined above suggest that the mechanism of action of the anthelmintic ponericins is disruption of cell membranes, similar to many hymenopteran venom peptides including melittin, the major component of honeybee venom. Many peptides that work by this mechanism of action adopt an α-helical structure in lipidic environments. The amphipathic nature of these helical peptides, with hydrophobic and charged patches that interact with the lipid tails and polar headgroups of phospholipids, respectively, is thought to underlie their ability disrupt biological membranes [37]. Helical wheel projections of the *Neoponera* peptides generated using NetWheels [35] revealed an asymmetric distribution of charged and hydrophobic residues which is a common feature of peptide toxins that disrupt biological membranes, suggesting that these five peptides may have a similar mechanism of action (Fig. 7D–I). Thus, we examined the secondary structure of anthelmintic ponericins in aqueous and lipidic environments using CD spectropolarimetry. CD spectra of the peptides in aqueous solution were typical of disordered protein chains, with a deep spectral minimum below 200 nm. Addition of 20% TFE or 20 mM SDS induced a radical change in the CD spectrum, with minima at 207 and 222 nm and a maximum at 193 nm, features that are characteristic of α-helical secondary structure [38] (Fig. 7A–C). These data suggest that the ponericins adopt an

α-helical conformation in membrane-mimetic environments, and further support the hypothesis that their primary mechanism of action is disruption of cell membranes.

3.3 Structure-activity relationships

The ponericins identified in this study are anthelmintic, antimicrobial and insecticidal. However, we have shown that they are also cytotoxic, hemolytic, activate mammalian sensory neurons, and induce pain behaviour *in vivo.* If these peptides are to find utility as commercial anthelmintics, antimicrobials or insecticides it will be necessary to remove or minimise their cytotoxic and algogenic activities. Thus, we performed a structure-activity relationship (SAR) study to provide a possible foundation for future rational engineering of therapeutically useful ponericins.

The contrasting bioactivity profiles of Nc3a and Nc3b, despite their 77% sequence identity, provided an ideal opportunity to generate a series of analogues to explore how the small number of sequence differences might contributed to their contrasting bioactivities. We therefore synthesised five Nc3b analogues by systematically substituting each of the five non-conservative substituted residues from Nc3a into Nc3b, to give [1A-]Nc3b, [T3W]Nc3b, [L19P]Nc3b, [G20E]Nc3b, and [S32R]Nc3b. A sixth analogue was synthesised in which all three conserved substitutions were swapped into Nc3b ([E5D, M21I, L39I]Nc3b, henceforth called [swap]Nc3b). Analogue sequences are shown in Figure 8A.

CD spectropolarimetry was used to confirm that the Nc3b analogues form α-helices in lipid-mimic environments, as observed for the native ponericins. All Nc3b analogues showed a tendency to disordered structure in water and α-helical conformations in lipid-mimetic environments (20 mM SDS and 20% TFE, Fig. 8D–F). We then performed anthelmintic, insecticidal, cytotoxicity, hemolysis and sensory neuron activation experiments and calculated the selectivity index (ratio of EC_{50} values on *H. contortus* compared to mammalian cells) for

each analogue. We found that all of these activities were closely correlated (summarised in Table 4), again supporting non-specific membrane perturbation as the mechanism of action of this class of peptides. Analogues [T3W]Nc3b and [S32R]Nc3b showed a moderate improvement in anthelmintic activity (IC_{50} 16.6–23.5 µM, Fig. 8B) and insecticidal activity (PD_{50} 1.1–2.5 nmol g^{-1}, Fig. 8C) relative to Nc3b, indicating that the substituted residues are functionally important. This was correlated with activation of DRG neurons and activity on F11 cells in fluorescent Ca^{2+} signalling assays (EC_{50} 12–25 µM, Fig. 8G). In contrast, analogues [G20E]Nc3b and [L19P]Nc3b showed a decrease in anthelmintic and insecticidal activity relative to Nc3a and Nc3b (Table 4). With the exception of [T3W]Nc3b (CC_{50} 16.9 µM), all analogues showed a reduction in cytotoxicity relative to Nc3a (CC_{50} >100 µM) and all were inactive against human erythrocytes (HC_{50} >100 µM, Table 4). Selectivity indices were estimated for each analogue as the ratio of EC_{50} for mammalian cell lines to the IC_{50} for inhibition of larval development (Fig. 8J). In general, the close correlation between anthelmintic activity and cell line activity resulted in selectivity indices below 10, with the greatest window observed for anthelmintic activity versus hemolysis.

4 Discussion

New anthelmintic agents (i.e. drugs that target parasitic helminths) are much needed due to rising drug resistance, dose-limiting side-effects and, in many cases, limited efficacy [14]. Several antiparasitic compounds have been isolated from ant venoms, such as the anti-trypanosomal dinoponeratoxins [12], but few studies have explored the activity of ant venoms against pathogenic nematodes. Here, by screening venoms against the blood-feeding nematode *H. contortus*, we isolated four novel anthelmintic ponericins from venom of the neotropical ant *N. commutata,* along with the previously identified but uncharacterised ponericin Na1b from the venom of *N. apicalis* [2].

552 The ponericins are a large family of peptides found in venom of ants in the genus
553 *Neoponera* (formerly *Pachycondyla*). They are members of the much larger superfamily of
554 aculeatoxins that are common in hymenopteran venoms [24]. The ponericins have been divided
555 into three subfamilies according to their sequence similarity and predominant N-terminal
556 amino acid residue: melittin-like W peptides; dermaseptin-like L peptides; and cecropin-like
557 G peptides [2, 19]. The novel ponericins identified in this study span all three subfamilies:
558 Na1b and Nc1a in subfamily W; Nc2a in subfamily L; and Nc3a and Nc3b in subfamily G
559 (Fig. 3). Similar to other ponericins, and the aculeatoxins in general [24], the peptides identified
560 in this study are short (25–31 residues), lack disulfide bridges, and are rich in lysine residues
561 that confer a net positive charge. These features are characteristic of many venom-derived
562 AMPs that disrupt cell membranes and are broadly cytolytic [39-41]; consistent with this
563 mechanism of action, we observed broad-spectrum activity for the ponericins across many cell
564 and tissue types (Table 3). In particular, Nc3a showed strong cytolytic effects, notably when
565 added to DRG cells (Fig. 6D). We therefore suggest that the full rational names for the
566 ponericins should include an "M" prefix that denotes membrane perturbation [3, 42].

567 The synthetic ponericins Na1b, Nc1a and Nc3a were found to inhibit *H. contortus*
568 development with an $IC_{50\ of}$ 2.8–5.6 µM, which is only 4–8-fold lower potency than the
569 commercial anthelmintic levamisole but considerably less active than macrocyclic lactone
570 anthelmintics [43, 44]. These ponericins have similar efficacy against *H. contortus* to
571 previously reported anthelmintic venom peptides, including the heterodimeric peptide Δ-
572 myrtoxin-Mp1a (Mp1a) from the Australian jack jumper ant *Myrmecia pilosula* (IC_{50} 6.8 µM)
573 [13] and the disulfide-rich inhibitor cystine knot (ICK) peptide U-LCTX-Dv_{33} (Dv33) from
574 venom of the Australian caterpillar *Doratifera vulnerans* (IC_{50} 2.6 µM) [45]. The disulfide-
575 rich cyclotide kalata B1, derived from the flowering plant *Oldenlandia affinis*, has similar
576 potency against *H. contortus* (IC_{50} 2.3 µM) [46]. Nc2a and Nc3b had moderate anthelmintic

activity (IC_{50} 23–38 µM), similar to the double-ICK peptide Hi1a from venom of the Australian funnel-web spider *Hadroncyhe infensa* (IC_{50} 22.9 µM) [27], and cecropin-like venom peptides from *D. vulnerans* (IC_{50} 24.5–30.5 µM) [45]. These cecropin-like peptides are similar to the ant-derived ponericins in that they are also short, lack disulfide-bridges, and disrupt membranes, conferring broad-spectrum activity against mammalian cells, helminths and microbes, and inducing nocifensive behaviour in mice [45]. Kalata B1 and Mp1a also exert anthelmintic activity via membrane disruption, and Mp1a induces spontaneous pain behaviour in mice [36, 46]. Subsequent SAR studies with Mp1a mirrored findings in this study in that anthelmintic, antimicrobial, cytotoxic, hemolytic and nocifensive activity are closely linked due to their common mechanism of membrane disruption [13, 36]. In contrast, the ICK-like *caterpillar* peptide Dv33 and the spider-venom peptide Hi1a appear to exert anthelmintic activity against *H. contortus* without membrane disruption, and do not induce nocifensive behaviour in rodents, so they may be better anthelmintic leads [27, 45, 47] Hence, while there has been substantial research focused on anthelmintic discovery from plant-derived natural products (for a recent review see [48]), this study adds to a growing body of evidence that venom peptides are an underexplored resource for anthelmintic discovery [49].

We also screened the ponericins for anthelmintic potential against *B. malayi*, a causative agent of human lymphatic filariasis and a model for filarial worm diseases. Nc3a and Nc3b produced only moderate effects on *B. malayi* worms, and these effects were time-dependent, with Nc1a initially inducing hypermotility followed by a reduction in motility. These effects require further characterisation to fully understand their biological significance. The observed difference in potency of the ponericins against *H. contortus* and *B. malayi* could be attributed to species-based variation and emphasises the importance of nematode-specific anthelmintic research.

It seems unlikely that the ponericins evolved in response to selection for anthelmintic activity. Instead, they are likely to have evolved for use in prey capture and/or defense from predators. In support of this hypothesis, we found that the ponericins are insecticidal and induce pain in mammals. Injection of ponericins into sheep blowflies induced rapid contractile paralysis that largely reversed over time. These results align with studies of the insecticidal activity of whole neoponeran venoms, which induce rapid, reversible paralysis or slow, permanent paralysis and death in a dose-dependent manner [7]. This was exemplified by Na1b, Nc2a and Nc3b, which showed moderate paralytic activity (PD_{50} values 25.8–38.1 nmol g^{-1}) but high doses (>100 nmol g^{-1}) failed to achieve 50% lethality. Similarly, peptide PONTX-Ae1a from venom of the predatory ant *Anochetus emarginatus* [50] and venom peptides from *Manica rubida* induce rapid paralysis in blowflies but are not lethal [51]. The exception in this study was Nc3a, which had similar PD_{50} and LD_{50} values and was the most active peptide tested; its LD_{50} (3.5 ± 0.9 nmol g^{-1}) is similar to peptide Δ-PSDTX-Pp1a isolated from the venom of *Pseudomyrmex penetrator* (LD_{50} 3 nmol g^{-1} in *L .cuprina*) [52], and considerably higher than previously reported values for other insecticidal G-subfamily ponericins, such as ponericin G1 (LD_{50} 25.7 nmol g^{-1} in *Acheta domestica*, [19]). Overall, the current study aligns with previous work indicating that both W and G-subfamily peptides have insecticidal activity [19], and the moderate paralytic activity of Nc2a indicates that insecticidal activity extends to L-subfamily ponericins as well. *N. commutata* are reported to be specialised termite predators [53], but the present study indicates that *N. commutata* ponericins are toxic at least to dipteran insects, indicating that the venom is active against at least two insect orders, Diptera and Blattodea. In future studies it would be interesting to test the *N. commutata*-derived ponericins against termites, and to explore activity against pest insect species.

Neoponeran ant venoms are extremely painful to humans, with stings from *N. commutata* compared to "the debilitating pain of a migraine contained in the tip of your

finger" [54]. The authors of this study note from personal experience that *N. commutata* and *N. apicalis* stings cause immediate sharp pain, which only lasts a few minutes. This painful sting has been utilised by several Amazonian tribes, including the Ka'apor, Wayapi and Wayana peoples, as part of puberty rituals wherein the ants are tied by the thorax into a necklace and placed on the chest and shoulders of recently pubescent girls similar to the infamous male puberty rituals where boys insert their hands into gloves woven with bullet ants, *Paraponera clavata* [55]. The identified ponericins are major components of *N. commutata* venom, and therefore we hypothesised that they contribute to the painful stings of these ants.

Application of ponericins to DRG cells indicated that Na1b, Nc1a and Nc3a induced a rapid increase in $[Ca^{2+}]_i$, consistent with activation of sensory neurons. The effect appeared to be driven, at least in part, by membrane disruption, as a corresponding increase in fluorescence was observed in the extracellular medium over time, indicating dye leakage due to pore formation or cytolysis. This was most prominently observed for Nc1a (Fig. 6). This sharp increase in fluorescence followed by rapid dye leakage was also observed in both F11 and HEK293 cells in a fluorescent Ca^{2+} assay, with no significant differences between the minimum effective concentrations in either cell line for Na1b and Nc1a. This suggested that these peptides act via a cell membrane disruption mechanism, rather than ion channel modulation or activation of neuron-specific receptors. Consistent with the ponericins activating sensory neurons, we found they induced nocifensive behaviour when injected intraplantar in mice. These effects were rapidly reversible, as is the pain associated with human envenomation by these ants. Our findings are consistent with observations on other cytolytic ant-venom peptides that disrupt neuronal cell membranes and induce spontaneous pain in mice, such as Mp1a [13, 36] and $MIITX_2$-Mg1a [24] from *Myrmecia* ant venoms. This is the first report of ponericins inducing pain, and we propose that the algogenic properties of G and W-subfamily

650 ponericins serve as a defense against predators, including mammals, and that pain induction
651 may be a key ecological function of cytolytic ant-venom peptides more broadly.

652 The membrane-perturbing properties of the anthelmintic ponericins also confers them
653 with antimicrobial activity. Ponericins were originally isolated from *N. goeldii* as peptides with
654 antimicrobial, hemolytic and insecticidal activities [19]. All ponericins in the present study,
655 with the exception of Nc3b, were active against Gram-positive and Gram-negative bacteria.
656 Na1b, Nc1a and Nc3a were the most potent antimicrobial peptides, with MICs in the low
657 micromolar range (0.18–5.9 μM). Our results align with previous observations that the G- and
658 W-subfamily ponericins are antimicrobial [19], though they are less potent than other ant
659 venom-derived antimicrobial peptides such as Mp1a [36]. We found that antimicrobial and
660 anthelmintic activity of the ponericins was generally correlated with their activity on
661 mammalian cells, including sensory neurons, HEK293 cells, and erythrocytes (Table 3). The
662 ponericins were typically less active on red blood cells, with 100 μM Nc2a, Nc3a and Nc3b
663 inducing no hemolysis. These results agree with previous work indicating that G- and L-
664 subfamily ponericins are not hemolytic [19], but W-subfamily ponericins are, as observed for
665 Nc1a and Na1b in this study (HC_{50} 28–60 μM).

666 The current study indicates that the taxonomic and cell-type selectivity of the ponericins
667 will need to be considerably improved if they are to serve as anthelmintic or antimicrobial leads.
668 We therefore undertook preliminary SAR studies with a view to identifying substitutions that
669 might enhance selectivity. Nc3a and Nc3b have similar primary structures (77% sequence
670 identity) but contrasting bioactivity profiles, prompting us to explore the relative contributions
671 of the differing residues to their bioactivities. No single substitution restored the activity of
672 Nc3b to Nc3a, indicating that there are additive contributions from all of the substituted
673 residues. CD spectropolarimetry indicated that all of the analogues form α-helices in lipid-
674 mimetic environments, suggesting that the observed differences in bioactivity are due to the

substituted residues rather than structural alterations. As with the parent ponericins, there was a general correlation in activity across all bioassays (Table 4), again supporting non-specific membrane disruption as a mechanism of action. For example, the analogue [T3W]Nc3b showed a two-fold improvement in anthelmintic activity (IC_{50} 16 μM) and 24-fold improvement in insecticidal activity (PD_{50} 1.1 nmol g^{-1}) over Nc3b, but about 10-fold increase in cytotoxicity. Previous work has indicated that tryptophan substitutions can improve AMP binding to the interfacial layer of membranes [56], which may explain this increase in activity. Likewise, [S32R]Nc3b showed a 10-fold improvement in insecticidal activity, with a corresponding approximately 10-fold decrease in the effective concentration for activation of F11 cells, reducing selectivity. The addition of arginine increased the net charge of the peptide relative to Nc3a and Nc3b (from +2 to +3), potentially facilitating binding of [S32R]Nc3b to cell membranes. In contrast, the analogue [G20E]Nc3b had a reduced net charge (+1) and an interrupted charge distribution relative to Nc3a and Nc3b, which may explain its loss of bioactivity (Table 4). Net charge has been shown to be important for the activity of many AMPs, including ponericin L1 [57]. [L19P]Nc3b also showed reduced efficacy relative to both Nc3a and Nc3b. The introduction of a proline residue may have introduced a bend in the peptide and increased its flexibility, thereby affecting its membrane-binding ability. However, the proline in this position is widely conserved across the broader ponericin G-subfamily (Fig. 3), suggesting that is an important structural feature for G-subfamily ponericins. More detailed exploration of SAR in future studies might facilitate rational engineering of ponericins with improved selectivity.

In conclusion, our data indicate that the ponericins possess a remarkably broad spectrum of activity — they are anthelmintic, insecticidal, algogenic, cytotoxic, hemolytic and antimicrobial. This broad-spectrum activity appears to be derived from their ability to non-specifically disrupt cell membranes, which confers both predatory and defensive functions for

these peptides in neoponeran ant venoms. The multifunctional nature of the ponericins may explain why they are the dominant components of *N. commutata* venom and are broadly distributed across the *Neoponera* genus. The pain-inducing activity of these peptides leads to a cautionary note: screening for unwanted cytotoxic and/or algogenic activity should always be considered when evaluating venom-derived AMPs as therapeutic leads. To this end, we have highlighted some differences in cell and tissue-type selectivity, which warrant further exploration to inform potential development of the ponericins for therapeutic applications.

Acknowledgments

We gratefully acknowledge the support of Geoff Brown and Steven Rice (Department of Agriculture and Fisheries, Ecoscience Precinct, Queensland) for culture and provision of *L .cuprina* maggots. We thank the Community for Open Access Antibiotic Discovery (Institute for Molecular Bioscience (IMB), The University of Queensland (UQ)) for performing antimicrobial, cytotoxicity and hemolytic assays. Special thanks to Mr Olivier Cheneval and Ms Poanna Tran for automated peptide assembly. We thank Associate Professor Bryan Fry (UQ), Dr Kate Baumann (UQ) and Dr Markus Muttenhaler (IMB, UQ) for supplying wasp venoms. We thank the IMB Sequencing Facility and Dr Alun Jones (IMB, UQ) for technical support and advice on mass spectrometry. We thank Dr Alex Wild (University of Texas at Austin, TX, USA) for photographs of *Neoponera commutata* and *N. apicalis.* This work was supported by the Westpac Bicentennial Foundation (Westpac Future Leaders Scholarship to S.A.N.), the Australian National Health and Medical Research Council (Project Grant APP1080405 to C.I.S; Principal Research Fellowship APP1136889 to G.F.K.), and the Australian Research Council (Future Fellowships FT160100055 and FT190100482 to C.I.S and V.H., respectively; Discovery Project DP200102867 to A.A.W, and DP190103787 to G.F.K, S.D.R., and I.V.,; and Centre of Excellence Grant CE200100012 to G.F.K.). E.A.B.U

was supported by a Norwegian Research Council FRIPRO-YRT Fellowship no. 287462. A.T was supported by “Investissement d'Avenir” grant ANR-10-LABX-25-01from Agence Nationale de la Recherche and a “Fonds européen de développement regional” grant GY0013708. Collection of ant species in French Guiana have been subjected to a declarative procedure (NOR: TREL1734890A/27) for non-commercial use at the competent administrative authority, in accordance with Article L.412-7 of the French environmental code. A.J.A was supported by a UQ PhD Scholarship.

Declaration of Competing Interest

The authors declare that they have no known competing financial interests or personal relationships that could have appeared to influence the work reported in this paper.

References

[1] R.S. Peters, L. Krogmann, C. Mayer, A. Donath, S. Gunkel, K. Meusemann, A. Kozlov, L. Podsiadlowski, M. Petersen, R. Lanfear, P.A. Diez, J. Heraty, K.M. Kjer, S. Klopfstein, R. Meier, C. Polidori, T. Schmitt, S. Liu, X. Zhou, T. Wappler, J. Rust, B. Misof, O. Niehuis, Evolutionary history of the Hymenoptera, Curr. Biol. 27 (2017) 1013–1018.

[2] S.R. Aili, A. Touchard, P. Escoubas, M.P. Padula, J. Orivel, A. Dejean, G.M. Nicholson, Diversity of peptide toxins from stinging ant venoms, Toxicon 92 (2014) 166-178.

[3] A. Touchard, S.R. Aili, E.G.P. Fox, P. Escoubas, J. Orivel, G.M. Nicholson, A. Dejean, The biochemical toxin arsenal from ant venoms, Toxins 8 (2016) 30.

[4] O. Otti, S. Tragust, H. Feldhaar, Unifying external and internal immune defences, Trends Ecol. Evol. 29 (2014) 625–634.

[5] E.G. LeBrun, P.J. Diebold, M.R. Orr, L.E. Gilbert, Widespread chemical detoxification of alkaloid venom by formicine ants, J. Chem. Ecol. 41 (2015) 884–895.

[6] J.O. Schmidt, Pain and lethality induced by insect stings: an exploratory and correlational study, Toxins 11 (2019) 11.

[7] J. Orivel, A. Dejean, Comparative effect of the venoms of ants of the genus *Pachycondyla* (Hymenoptera: Ponerinae), Toxicon 39 (2001) 195–201.

[8] J.R.A. dos Santos-Pinto, A. Perez-Riverol, A.M. Lasa, M.S. Palma, Diversity of peptidic and proteinaceous toxins from social Hymenoptera venoms, Toxicon 148 (2018) 172–196.

[9] A. Rifflet, S. Gavalda, N. Téné, J. Orivel, J. Leprince, L. Guilhaudis, E. Génin, A. Vétillard, M. Treilhou, Identification and characterization of a novel antimicrobial peptide from the venom of the ant *Tetramorium bicarinatum*, Peptides 38 (2012) 363–370.

[10] I. Zelezetsky, U. Pag, N. Antcheva, H.-G. Sahl, A. Tossi, Identification and optimization of an antimicrobial peptide from the ant venom toxin pilosulin, Arch. Biochem. Biophys. 434 (2005) 358–364.

[11] J.F.C. Vinhote, D.B. Lima, R.R.P.P.B de Menezes, C.P. Mello, B.M. de Souza, A. Havt, M.S. Palma, R.P. dos Santos, E.L. de Albuquerque, V.N. Freire, A.M.C. Martins, Trypanocidal activity of mastoparan from *Polybia paulista* wasp venom by interaction with TcGAPDH, Toxicon 137 (2017) 168–172.

[12] D.B. Lima, C.P. Mello, I.C.J. Bandeira, R.R.P. P.B. de Menezes, T.L. Sampaio, C.B. Falcão, J.R.L. Morlighem, G. Rádis-Baptista, A.M.C. Martins, The dinoponeratoxin peptides from the giant ant *Dinoponera quadriceps* display *in vitro* antitrypanosomal activity, Biol. Chem. 399 (2018) 187–196.

[13] S.A. Nixon, Z. Dekan, S.D. Robinson, S. Guo, I. Vetter, A.C. Kotze, P.F. Alewood, G.F. King, V. Herzig, It takes two: dimerization is essential for the broad-spectrum predatory and defensive activities of the venom peptide Mp1a from the jack jumper ant *Myrmecia pilosula*, Biomedicines 8 (2020) 185.

[14] S.A. Nixon, C. Welz, D. Woods, L. Costa-Junior, M. Zamanian, R. Martin, Where are all the anthelmintics? Challenges and opportunities on the path to new anthelmintics, Int. J. Parasitol.: Drugs Drug Resist. (2020) 8–16.

[15] R.M. Kaplan, A.N. Vidyashankar, An inconvenient truth: global worming and anthelmintic resistance, Vet. Parasitol. 186 (2012) 70–78.

[16] T.G. Geary, Chapter 10: *Haemonchus contortus*: applications in drug discovery, in: R.B. Gasser, G.V. Samson-Himmelstjerna (Eds.), Advances in Parasitology, Academic Press 2016, pp. 429–463.

[17] J. Charlier, L. Rinaldi, V. Musella, H.W. Ploeger, C. Chartier, H.R. Vineer, B. Hinney, G. von Samson-Himmelstjerna, B. Băcescu, M. Mickiewicz, T.L. Mateus, M. Martinez-Valladares, S. Quealy, H. Azaizeh, B. Sekovska, H. Akkari, S. Petkevicius, L. Hektoen, J. Höglund, E.R. Morgan, D.J. Bartley, E. Claerebout, Initial assessment of the economic burden of major parasitic helminth infections to the ruminant livestock industry in Europe, Prev. Vet. Med. 182 (2020) 105103.

[18] J. Lane, T. Jubb, R. Shephard, J. Webb-Ware, G. Fordyce, MLA final report: priority list of endemic diseases for the red meat industries, Sydney, 2015.

[19] J. Orivel, V. Redeker, J.P. Le Caer, F. Krier, A.M. Revol-Junelles, A. Longeon, A. Chaffotte, A. Dejean, J. Rossier, Ponericins, new antibacterial and insecticidal peptides from the venom of the ant *Pachycondyla goeldii*, J. Biol. Chem. 276 (2001) 17823–17829.

[20] C.T. Cologna, R.S. Rodrigues, J. Santos, E. de Pauw, E.C. Arantes, L. Quinton, Peptidomic investigation of *Neoponera villosa* venom by high-resolution mass spectrometry: seasonal and nesting habitat variations, J. Venom. Anim. Toxins Incl. Trop. Dis. 24 (2018) 6.

[21] H.V. Dodou Lima, C.S. de Paula Cavalcante, G. Rádis-Baptista, Antifungal *in vitro* activity of pilosulin- and ponericin-like peptides from the giant ant *Dinoponera quadriceps* and synergistic effects with antimycotic drugs, Antibiotics 9 (2020) 354.

[22] A.F.C. Torres, C. Huang, C.-M. Chong, S.W. Leung, A.R.B. Prieto-da-Silva, A. Havt, Y.P. Quinet, A.M.C. Martins, S.M.Y. Lee, G. Rádis-Baptista, Transcriptome analysis in venom gland of the predatory giant ant *Dinoponera quadriceps*: insights into the polypeptide toxin arsenal of hymenopterans, PloS One 9 (2014) e87556-e87556.

[23] K.A. Pluzhnikov, S.A. Kozlov, A.A. Vassilevski, O.V. Vorontsova, A.V. Feofanov, E.V. Grishin, Linear antimicrobial peptides from *Ectatomma quadridens* ant venom, Biochimie 107 (2014) 211–215.

[24] S.D. Robinson, A. Mueller, D. Clayton, H. Starobova, B.R. Hamilton, R.J. Payne, I. Vetter, G.F. King, E.A.B. Undheim, A comprehensive portrait of the venom of the giant red bull ant, *Myrmecia gulosa*, reveals a hyperdiverse hymenopteran toxin gene family, Sci. Adv. 4 (2018) eaau4640.

[25] G.A. Albers, S.K. Burgess, Serial passage of *Haemonchus contortus* in resistant and susceptible sheep, Vet. Parasitol. 28 (1988) 303–306.

[26] A.C. Kotze, J. O'Grady, J. Emms, A.F. Toovey, S. Hughes, P. Jessop, M. Bennell, P.E. Vercoe, D.K. Revell, Exploring the anthelmintic properties of Australian native shrubs with respect to their potential role in livestock grazing systems, Parasitology 136 (2009) 1065–1080.

[27] S.A. Nixon, N.J. Saez, V. Herzig, G.F. King, A.C. Kotze, The antitrypanosomal diarylamidines, diminazene and pentamidine, show anthelmintic activity against *Haemonchus contortus in vitro*, Vet. Parasitol. 270 (2019) 40–46.

[28] A.J. Agwa, N. Lawrence, E. Deplazes, O. Cheneval, R.M. Chen, D.J. Craik, C.I. Schroeder, S.T. Henriques, Spider peptide toxin HwTx-IV engineered to bind to lipid membranes has an increased inhibitory potency at human voltage-gated sodium channel $hNa_V1.7$, Biochim. Biophys. Acta – Biomembranes 1859 (2017) 835–844.

[29] A.J. Agwa, L.V. Blomster, D.J. Craik, G.F. King, C.I. Schroeder, Efficient enzymatic ligation of inhibitor cystine knot spider venom peptides: using sortase A to form double-knottins that probe voltage-gated sodium channel $Na_V1.7$, Bioconjug. Chem. 29 (2018) 3309–3319.

[30] A.J. Agwa, S. Peigneur, C.Y. Chow, N. Lawrence, D.J. Craik, J. Tytgat, G.F. King, S.T. Henriques, C.I. Schroeder, Gating modifier toxins isolated from spider venom: modulation of voltage-gated sodium channels and the role of lipid membranes, J. Biol. Chem. 293 (2018) 9041–9052.

[31] B. Storey, C. Marcellino, M. Miller, M. Maclean, E. Mostafa, S. Howell, J. Sakanari, A. Wolstenholme, R. Kaplan, Utilization of computer processed high definition video imaging for measuring motility of microscopic nematode stages on a quantitative scale: “The Worminator”, Int. J. Parasitol. Drugs Drug Resist. 4 (2014) 233–243.

[32] C. Marcellino, J. Gut, K.C. Lim, R. Singh, J. McKerrow, J. Sakanari, WormAssay: a novel computer application for whole-plate motion-based screening of macroscopic parasites, PLOS Negl. Trop. Dis. 6(2012) e1494.

[33] S. Guo, V. Herzig, G.F. King, Dipteran toxicity assays for determining the oral insecticidal activity of venoms and toxins, Toxicon 150 (2018) 297–303.

[34] V. Herzig, W.C. Hodgson, Neurotoxic and insecticidal properties of venom from the Australian theraphosid spider *Selenotholus foelschei*, Neurotoxicology 29 (2008) 471–475.

[35] A.R. Mól, M.S. Castro, W. Fontes, NetWheels: a web application to create high quality peptide helical wheel and net projections, bioRxiv (2018) 416347.

[36] Z. Dekan, S.J. Headey, M. Scanlon, B.A. Baldo, T.-H. Lee, M.-I. Aguilar, J.R. Deuis, I. Vetter, A.G. Elliott, M. Amado, M.A. Cooper, D. Alewood, P.F. Alewood, Δ-Myrtoxin-Mp1a is a helical heterodimer from the venom of the jack jumper ant that has antimicrobial, membrane-disrupting, and nociceptive activities, Angew. Chem. Int. Ed. 56 (2017) 8495–8499.

[37] M.-T. Lee, T.-L. Sun, W.-C. Hung, H.W. Huang, Process of inducing pores in membranes by melittin, Proc. Natl. Acad. Sci. USA 110 (2013) 14243–14248.

[38] T.H. Szeto, S.L. Rowland, C.L. Habrukowich, G.F. King, The MinD membrane targeting sequence is a transplantable lipid-binding helix, J. Biol. Chem. 278 (2003) 40050–40056.

[39] L. Kuhn-Nentwig, Antimicrobial and cytolytic peptides of venomous arthropods, Cell. Mol. Life Sci. 60 (2003) 2651–2668.

[40] D.E. Schlamadinger, J.E. Gable, J.E. Kim, Toxins and antimicrobial peptides: interactions with membranes, Proc. SPIE Int. Soc. Opt. Eng. 7397 (2009) 73970J.

[41] L. Kuhn-Nentwig, J. Willems, T. Seebeck, T. Shalaby, M. Kaiser, W. Nentwig, Cupiennin 1a exhibits a remarkably broad, non-stereospecific cytolytic activity on bacteria, protozoan parasites, insects, and human cancer cells, Amino Acids 40 (2011) 69–76.

[42] G.F. King, M.C. Gentz, P. Escoubas, G.M. Nicholson, A rational nomenclature for naming peptide toxins from spiders and other venomous animals, Toxicon 52 (2008) 264-76.

[43] A.C. Kotze, A. Ruffell, J. Lamb, T.P. Elliott, Response of drug-susceptible and -resistant *Haemonchus contortus* larvae to monepantel and abamectin alone or in combination *in vitro*, Vet. Parasitol. 249 (2018) 57–62.

[44] A. Raza, J. Lamb, M. Chambers, P.W. Hunt, A.C. Kotze, Larval development assays reveal the presence of sub-populations showing high- and low-level resistance in a monepantel (Zolvix®)-resistant isolate of *Haemonchus contortus*, Vet. Parasitol. 220 (2016) 77–82.

[45] A.A. Walker, S.D. Robinson, J.-P.V. Paluzzi, D.J. Merritt, S.A. Nixon, C.I. Schroeder, J. Jin, M.H. Goudarzi, A.C. Kotze, Z. Dekan, A. Sombke, P.F. Alewood, B.G. Fry, M.E. Epstein, I. Vetter, G.F. King, Production, composition, and mode of action of the painful defensive venom produced by a limacodid caterpillar, *Doratifera vulnerans*, Proc. Natl. Acad. Sci. USA 118 (2021) e2023815118.

[46] M.L. Colgrave, A.C. Kotze, Y.-H. Huang, J. O'Grady, S.M. Simonsen, D.J. Craik, Cyclotides: natural, circular plant peptides that possess significant activity against gastrointestinal nematode parasites of sheep, Biochemistry 47 (2008) 5581–5589.

[47] I.R. Chassagnon, C.A. McCarthy, Y.K.Y. Chin, S.S. Pineda, A. Keramidas, M. Mobli, V. Pham, T.M. De Silva, J.W. Lynch, R.E. Widdop, L.D. Rash, G.F. King, Potent neuroprotection after stroke afforded by a double-knot spider-venom peptide that inhibits acid-sensing ion channel 1a, Proc. Natl. Acad. Sci. USA 114 (2017) 3750–3755.

[48] J.F. Garcia-Bustos, B.E. Sleebs, R.B. Gasser, An appraisal of natural products active against parasitic nematodes of animals, Parasit. Vectors 12 (2019) 306.

[49] V. Herzig, B. Cristofori-Armstrong, M.R. Israel, S.A. Nixon, I. Vetter, G.F. King, Animal toxins—Nature's evolutionary-refined toolkit for basic research and drug discovery, Biochem. Pharmacol. 181 (2020) 114096.

[50] A. Touchard, A. Brust, F.C. Cardoso, Y.K. Chin, V. Herzig, A.H. Jin, A. Dejean, P.F. Alewood, G.F. King, J. Orivel, P. Escoubas, Isolation and characterization of a structurally unique β-hairpin venom peptide from the predatory ant *Anochetus emarginatus*, Biochim. Biophys. Acta 1860 (2016) 2553–2562.

[51] A. Touchard, S.R. Aili, N. Téné, V. Barassé, C. Klopp, A. Dejean, R.M. Kini, Mrinalini, L. Coquet, T. Jouenne, B. Lefranc, J. Leprince, P. Escoubas, G.M. Nicholson, M. Treilhou, E. Bonnafé, Venom peptide repertoire of the European myrmicine ant *Manica rubida*: identification of insecticidal toxins, J. Proteome Res. 19 (2020) 1800–1811.

[52] A. Touchard, H.C. Mendel, I. Boulogne, V. Herzig, N. Braga Emidio, G.F. King, M. Triquigneaux, L. Jaquillard, R. Beroud, M. De Waard, O. Delalande, A. Dejean, M. Muttenthaler, C. Duplais, Heterodimeric insecticidal peptide provides new insights into the molecular and functional diversity of ant venoms, ACS Pharmacol. Trans. Sci. 3(6) (2020) 1211–1224.

[53] A.E. Mill, Predation by the ponerine ant *Pachycondyla commutata* on termites of the genus *Syntermes* in Amazonian rain forest, J. Nat. Hist. 18 (1984) 405–410.

[54] J.O. Schmidt, Sting of the Wild, John Hopkins University Press, Baltimore, 2016.

[55] W. Balée, Indigenous savoir faire: retention of traditional knowledge in *Cultural forests of the Amazon: a historical ecology of people and their landscapes*, The University of Alabama Press, Tuscaloosa, 2013, pp. 140–148.

[56] X. Feng, S. Jin, M. Wang, Q. Pang, C. Liu, R. Liu, Y. Wang, H. Yang, F. Liu, Y. Liu, The critical role of tryptophan in the antimicrobial activity and cell toxicity of the duck antimicrobial peptide DCATH, Front. Microbiol. 11 (2020) 1146.

[57] A.S. Senetra, M.R. Necelis, G.A. Caputo, Investigation of the structure-activity relationship in ponericin L1 from *Neoponera goeldii*, Peptide Sci. 112 (2020) e24162.

Figure Legends

Figure 1: Screen of crude hymenopteran venoms against drug-susceptible *H. contortus.* Bars show inhibition of larval development (relative to negative control) calculated from triplicate assays at each of the three indicated concentrations. Data are mean ± SEM.

Figure 2: Isolation of ponericins with anthelmintic activity from the venoms of *N. apicalis* and *N. commutata.* Chromatograms showing analytical RP-HPLC fractionation of crude venom from (A) *N. commutata* and (D) *N. apicalis,* with peaks containing anthelmintic activity highlighted. Insets show *N. commutata* and *N. apicalis* worker ants (photographs by Dr Alex Wild, The University of Texas at Austin, USA). (B, C, E–G) Successive purification by analytical RP-HPLC identified five anthelmintic ponericins. Insets are MALDI-TOF MS spectra showing the monoisotopic mass of each peptide. Amino acid sequences were determined using LC-MS/MS and compared against a draft venom-gland transcriptome for *N. commutata* and previously identified ponericins for *N. apicalis.* (H) An example mass spectrum showing ions leading to identification of the amino acid sequence for ponericin Nc2a.

Figure 3: Sequence alignments of anthelmintic and canonical ponericins. Nc1a, Nc2a, Nc3a and Nc3b, and Na1b show homology to the three described subfamilies of ponericins: W, L, and G. Ponericins identified in this study are shown in bold. Identity (%ID) and similarity (%Sim) are shown compared to canonical ponericins at the top of the alignment for each subfamily. Identical residues are highlighted in yellow, positively-charged residues (K and R) are coloured blue, and conservative substitutions are shown in red. Additional species included in the alignments are: *Apis flora, A. flora*; *Dinoponera quadriceps, D. quadriceps; Ectatomma brunneum, E. brunneum; Phasmahyla jandaia, P. jandaia; Antheraea pernyi, A. pernyi.*

Figure 4: Analytical RP-HPLC chromatograms and ESI-MS spectra of purified synthetic peptides. Calculated masses are shown adjacent to each mass spectrum.

Figure 5: Ponericins are active against parasitic nematodes and sheep blowflies. (A) Concentration-response curves for inhibition of the larval development of *H. contortus* by synthetic ponericins. Each data point represents mean ± SEM based on three experiments of triplicate assays. (B) Motility of adult male *B. malayi* (movements per minute normalised to control, MMU) after addition of synthetic ponericins over a 96 h timeframe. Points represent mean ± SEM from three independent experiments using four worms per dose (n = 12). Asterisks indicate significant differences, determined by one-way ANOVA with Dunnett's correction comparing ponericin-treated worms with untreated worms. (C–D) Dose-response curves for insecticidal effects of ponericins following microinjection into adult sheep blowflies (*L. cuprina*). Data are shown for paralysis at 1 h (C) and lethality at 24 h (D). Each data point represents the mean ± SEM for three experiments (n = 10 flies per dose, per experiment).

Figure 6: Ponericins perturb cell membranes *in vitro* and induce spontaneous pain behaviour *in vivo.* (A,D) Photomicrographs (20×) of DRG cells before and at 90 s and 120 s after application of 10 µM Na1b (A) and Nc1a (D). (B,E) Changes in intracellular calcium were measured as an increase in fluorescence relative to baseline ($\Delta F/F_0$), where each line represents an individual cell response. (C) Comparison of median effective concentration (EC_{50} values) observed in FLIPR assays for F11 and HEK293 cells for each peptide, calculated from concentration-response curves shown in (G,I,K,M), and compared via Student's *t*-tests with Welch's correction. Melittin was used as a positive control. (F, H, J, L) Fluorescence responses of F11 cells after addition of peptides Na1b, Nc1a, Nc3a and Nc3b over a range of concentrations (0.01–100 µM) recorded using a FLIPR. The corresponding concentration-

response curve is plotted adjacent to each fluorescence trace and was calculated from the change in fluorescence (ΔF) from the maximal response less baseline (n = 3). (N–P) Nocifensive behaviour in mice after injection of ponericins (30 µM). Asterisks indicate statistical significance ($p < 0.05$) (student's t-test with Welch's correction relative to vehicle). Error bars throughout the figure indicate SEM.

Figure 7: Ponericins adopt an α-helical conformation in lipid-like environments. CD spectra of synthetic ponericins (25 µM) dissolved in (A) ultrapure water, (B) 20% TFE, and (C) 20 mM SDS. α-Helical wheel projections generated using NetWheels [35] for (D) Na1b; (E) Nc1a; (F) Nc2a; (G) Nc3a (N-terminal, G1-P18); (H) Nc3a (C-terminal E19-N30); and (I) Nc3b. Two wheels are shown for Nc3a representing the regions either side of a proline residue, which is likely to disrupt helicity.

Figure 8: Characterisation of Nc3b analogues. (A) Sequence alignments of Nc3a and Nc3b with analogues. Positively charged residues are shown in blue, negatively charged residues are shown in purple, and amino acid substitutions in analogues are highlighted in pink. (B) Concentration-response curves for inhibition of *H. contortus* larval development by Nc3a, Nc3b, and active analogues. Each point represents mean ± SEM from three experiments of triplicate assays. (C) Dose-response curves for paralytic effects of Nc3a, Nc3b, and active analogues at 1 h after microinjection into *L. cuprina*. Each point represents mean ± SEM for three experiments (n = 10 flies per dose, per experiment). (D–F) CD spectra for Nc3a, Nc3b and analogues in (D) water, (E) 20% TFE, and (F) 20 mM SDS. (G) Photomicrograph (20×) of DRG cells before and at 90 s after application of 10 µM [T3W]Nc3b. (H) Corresponding increase in intracellular calcium in DRG cells after application of 10 µM [T3W]Nc3b measured as an increase in fluorescence relative to baseline ($\Delta F/F_0$), where each line represents an

individual cell response. (I) Concentration-response curves for activation of F11 cells in a FLIPR assay by Nc3a, Nc3b and selected analogues. (J) Selectivity index for Nc3a, Nc3b and analogues, calculated as EC_{50} of mammalian cell line divided by the IC_{50} for inhibition of *H. contortus* larval development.

5 Figures

Figure 1.

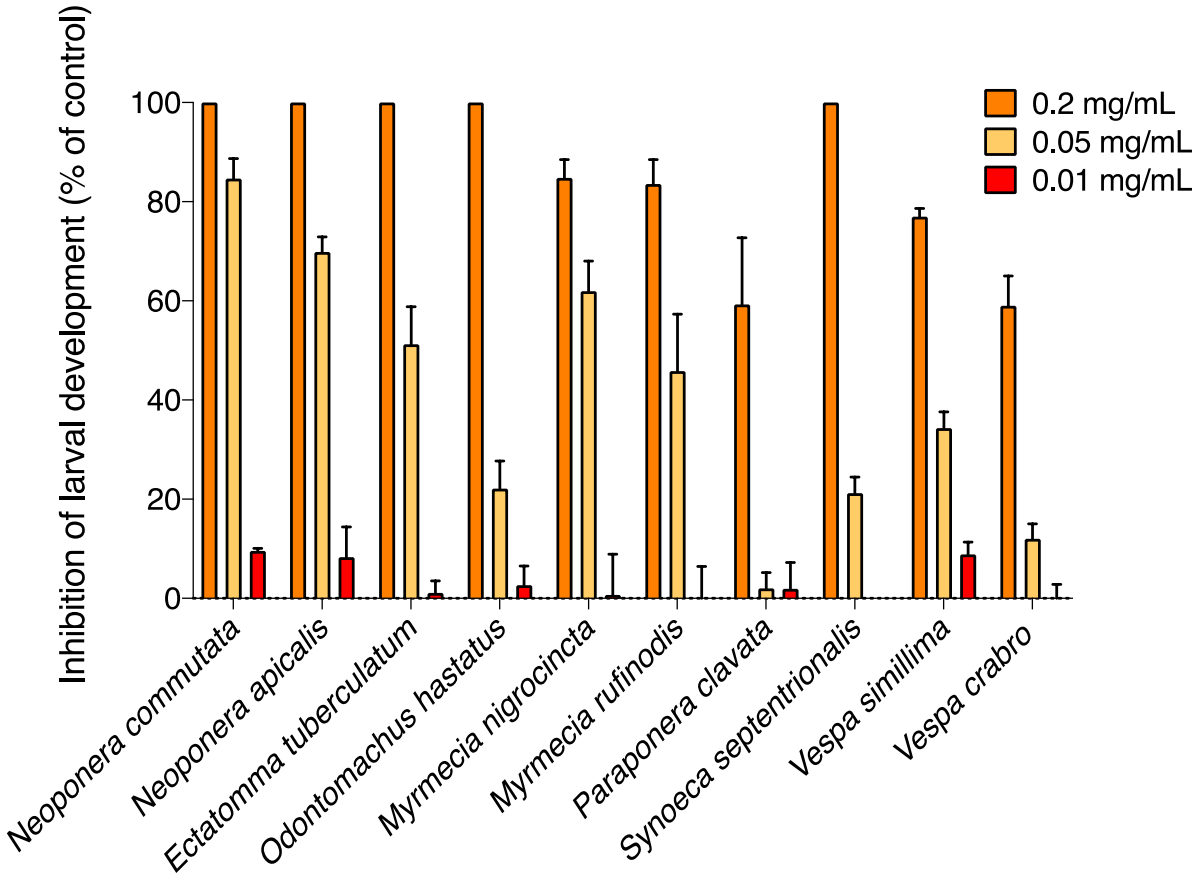

Figure 2.

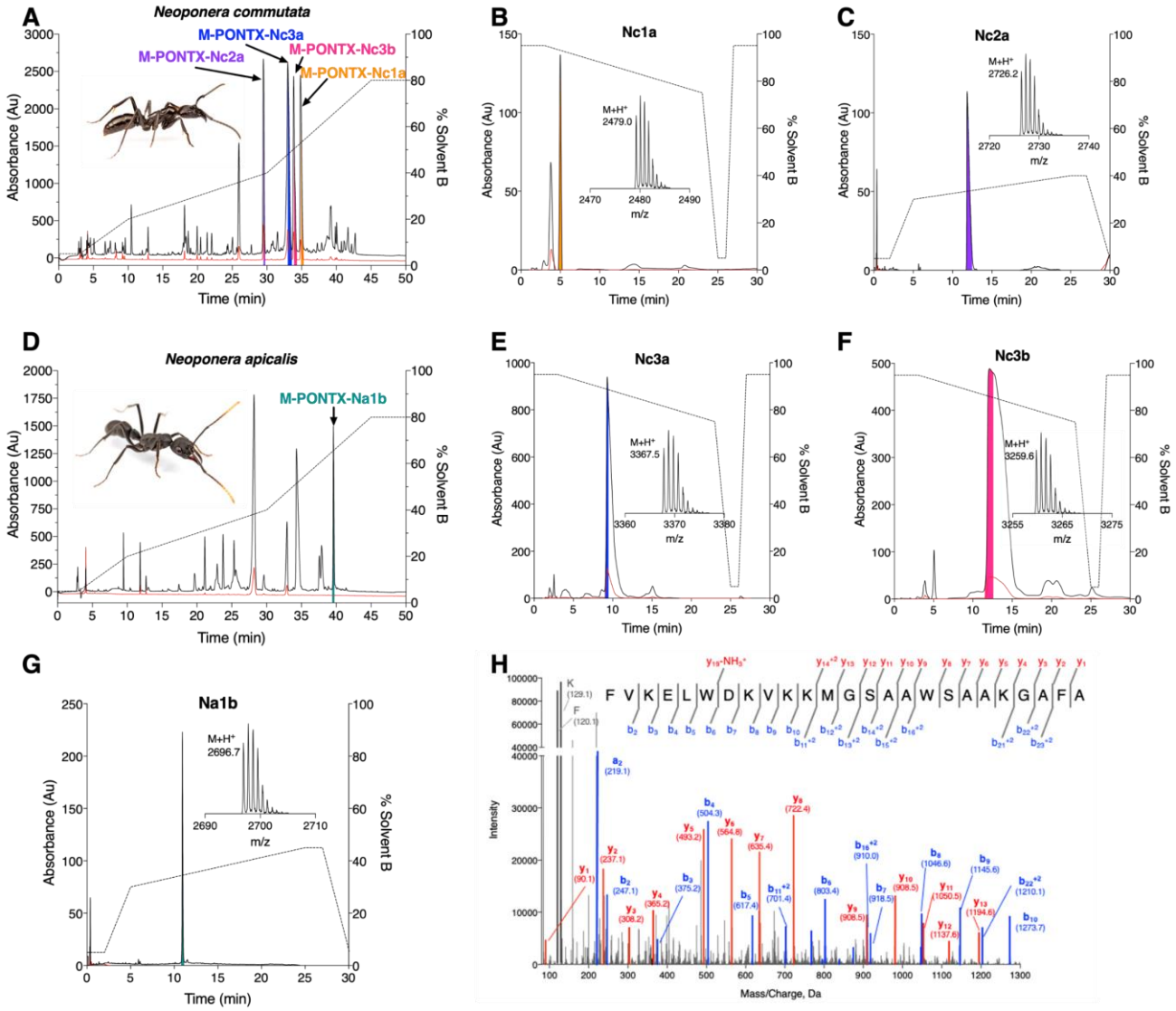
A
Neoponera commutata
M-PONTX-Nc3a
M-PONTX-Nc3b
M-PONTX-Nc2a
M-PONTX-Nc1a
Absorbance (Au)
% Solvent B
Time (min)
B
Nc1a
M+H+ 2479.0
m/z
C
Nc2a
M+H+ 2726.2
m/z
D
Neoponera apicalis
M-PONTX-Na1b
E
Nc3a
M+H+ 3367.5
m/z
F
Nc3b
M+H+ 3259.6
m/z
G
Na1b
M+H+ 2696.7
m/z
H
F V K E L W D K V K K M G S A A W S A A K G A F A
Intensity
Mass/Charge, Da

42

Figure 3.

Ponericin W-subfamily: 'melittin-like'

Species	Toxin	Common name	Sequence	Residue #	% ID	% Sim
N. goeldii	U-PONTX-Ng1a	Ponericin W1	-WLGSALKIGAKLLPSVVGLFKKKQ---	25	100	100
N. goeldii	U-PONTX-Ng1b	Ponericin W2	-WLGSALKIGAKLLPSVVGLFQKKK---	25	92	92
N. apicalis	**M-PONTX-Na1b**	**Ponericin Pa II 2**	-FLGALLKIGAKLLPSVVGLFKKKQQ---	25	84	88
N. apicalis	U-PONTX-Na1a	Ponericin Pa II 1	-FLGGLMKIGAKLLPSVIGLFKKKQ----	24	72	84
N. goeldii	U-PONTX-Ng1e	Ponericin W5	-FWGALIKGAAKLIPSVVGLFKKKQ----	24	60	75
N. goeldii	M-PONTX-Ng1d	Ponericin W4	GIWGTALKWGVKLLPKLVGMAQTKKQ---	26	54	65
N. goeldii	U-PONTX-Ng1c	Ponericin W3	GIWGTLAKIGIKAVPRVISMLKKKKQ---	26	46	65
N. inversa	U-PONTX-Ni1b	Ponericin Pi II 2	FLWGALIKGAGKLISRVVGSLKKKKQ---	26	46	65
N. goeldii	M-PONTX-Ng1f	Ponericin W6	-FIGTALG-IASAIPAIVKLFK-------	20	40	60
N. inversa	U-PONTX-Ni1a	Ponericin Pi II 1	-FIGAALG-ALTAIPSIIKLFK-------	20	32	60
N. commutata	**M-PONTX-Nc1a**	**Novel**	-FWGAAAKMLGKALPGLISMFQKN-----	23	32	60
A. flora	Melittin	Melittin	-GIGAVLKVLTTGLPALISWIKRKRQQ--	26	31	58
E. brunneum	M-ECTX-Eb2a	Ponericin-Q42	-FWGAVWKILSKVLPHIPGTVKWLQEKV-	27	30	52
E. brunneum	M-ECTX-Eb2c	Ponericin-Q50	-FWGALFKTVAKVVAPFVPDIVKWVQEKV	28	25	43
D. quadriceps	M-PONTX-Dq3a	Dq3a	-FWGTLAKWALKAIPAAMGMKQNK-----	23	24	60
E. brunneum	M-ECTX-Eb2b	Ponericin-Q49	-FWGALVAGLAPKVAIGIKWAINKKG---	25	16	48

Ponericin L-subfamily: 'dermaseptin-like'

N. goeldii	M-PONTX-Ng2b	Ponericin L2	LLKELWTKIKGAGKAVLGKI-KGLL-	24	100	100
N. goeldii	M-PONTX-Ng2a	Ponericin L1	LLKELWTKMKGAGKAVLGKI-KGLL-	24	96	100
N. inversa	U-PONTX-Ni2a	Ponericin Pi III 1	LLKELWKKIKGAGKAVLGKI-KGLL-	24	96	96
N. commutata	**M-PONTX-Nc2a**	**Novel**	FVKELWDKVKKMGSAAWSAA-KGAFA	25	40	60
P. jandaia	Dermaseptin-J6	Dermaseptin-J6	---GLWSKIKEAGKAAVKAAGKAALGAVADSV	29	40	60

Ponericin G-subfamily: 'cecropin-like'

N. goeldii	M-PONTX-Ng3a	Ponericin G1	-GWKDWAKKAGGWLKKKGPGMAKAALKAAMQ	30	100	100
N. inversa	U-PONTX-Ni3c	Ponericin Pi I3	-GWRDWLKKAGGWLKKKGPGILKAALGAATQ	30	83	90
N. goeldii	U-PONTX-Ng3c	Ponericin G3	-GWKDWLNKGKEWLKKKGPGIMKAALKAATQ	30	73	80
N. goeldii	U-PONTX-Ng3e	Ponericin G5	-GLKDWVKIAGGWLKKKGPGILKAAMAAATQ	30	73	80
N. inversa	U-PONTX-Ni3b	Ponericin Pi I2	-GWRDWLKKGKEWIKAKGPGIVKAALKAAVQ	30	67	80
N. goeldii	U-PONTX-Ng3b	Ponericin G2	-GWKDWLKKGKEWLKAKGPGIVKAALQAATQ	30	70	77
N. inversa	U-PONTX-Ni3a	Ponericin Pi I1	-GWRDWLNKGKEWLKKKGPGMVKAALAAATQ	30	70	77
N. inversa	U-PONTX-Ni3d	Ponericin Pi I4	-GWKDWLKTAGGWLKKKGPSILKAVVGAATQ	30	70	77
N. goeldii	M-PONTX-Ng3d	Ponericin G4	-DFKDWMKTAGEWLKKKGPGILKAAMAAAT-	29	63	73
N. apicalis	U-PONTX-Na3a	Ponericin Pa I1	-GFKDWMKKAGSWLKKKGPALIKAAMQE---	27	60	73
N. apicalis	U-PONTX-Na3b	Ponericin Pa I2	-GFMDLIKKAGGWLKKKGPALIKAALQE---	27	60	70
N. commutata	**M-PONTX-Nc3a**	**Novel**	-GWKDWLNKAKDFIKEKGPEILRAAANAAIN	30	50	73
N. commutata	**M-PONTX-Nc3b**	**Novel**	AGTKEWLNKAKDFIKEKGLGMLSAAANAALN	31	45	68
A. pernyi	Cecropin B	Cecropin B	-KWKIFKKIEKVGRNIRNGIIKAGPAVAVLGEAKAL	31	45	68

Figure 4.

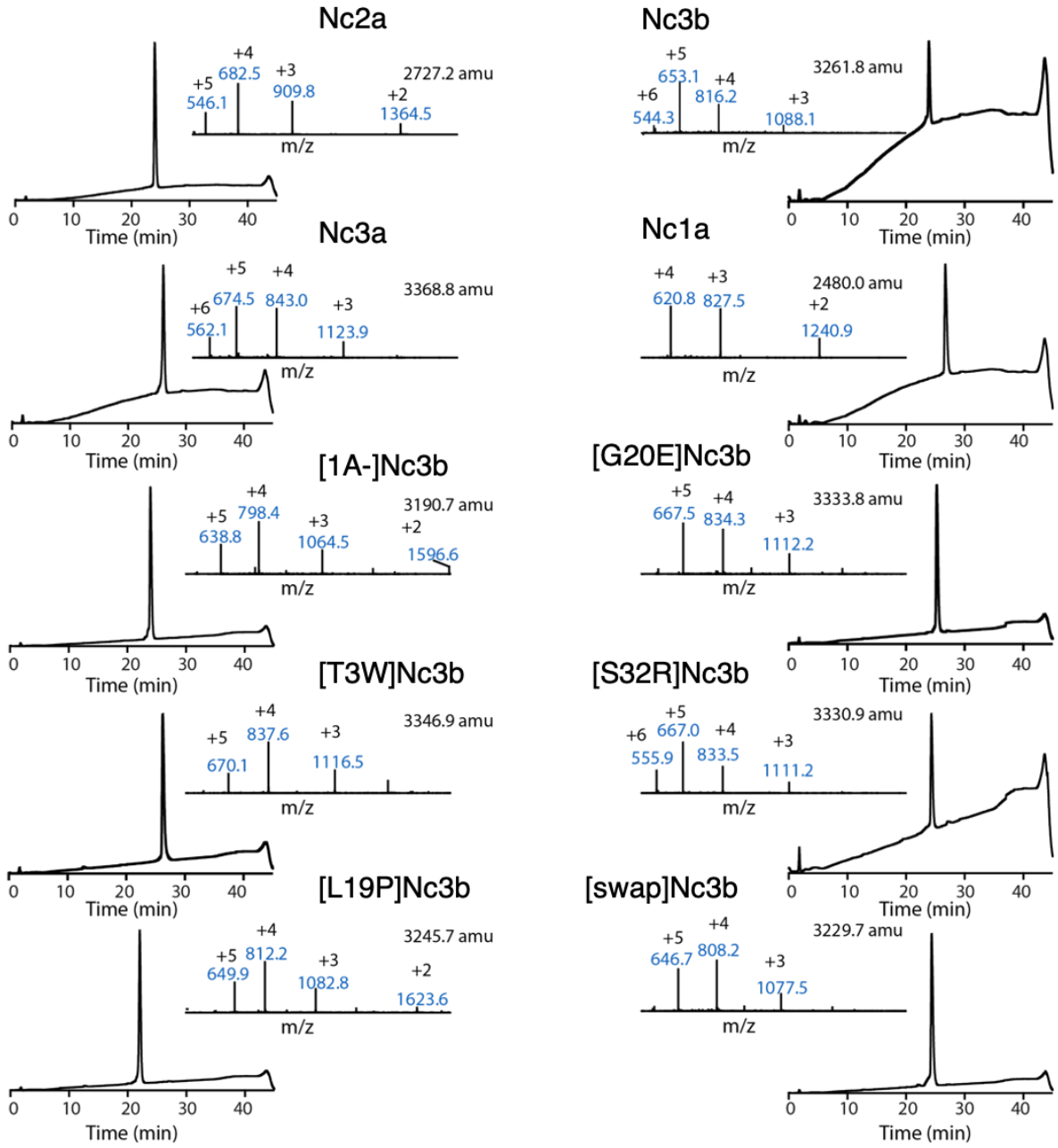
Nc2a
+4
682.5
+5
546.1
+3
909.8
+2
1364.5
2727.2 amu
m/z
Time (min)
Nc3b
+5
653.1
+6
544.3
+4
816.2
+3
1088.1
3261.8 amu
m/z
Time (min)
Nc3a
+5
+4
+6
674.5
843.0
562.1
+3
1123.9
3368.8 amu
m/z
Time (min)
Nc1a
+4
620.8
+3
827.5
+2
1240.9
2480.0 amu
m/z
Time (min)
[1A-]Nc3b
+4
+5
798.4
638.8
+3
1064.5
+2
1596.6
3190.7 amu
m/z
Time (min)
[G20E]Nc3b
+5
667.5
+4
834.3
+3
1112.2
3333.8 amu
m/z
Time (min)
[T3W]Nc3b
+4
+5
837.6
670.1
+3
1116.5
3346.9 amu
m/z
Time (min)
[S32R]Nc3b
+5
+6
667.0
555.9
+4
833.5
+3
1111.2
3330.9 amu
m/z
Time (min)
[L19P]Nc3b
+4
+5
812.2
649.9
+3
1082.8
+2
1623.6
3245.7 amu
m/z
Time (min)
[swap]Nc3b
+5
646.7
+4
808.2
+3
1077.5
3229.7 amu
m/z
Time (min)

Figure 5.

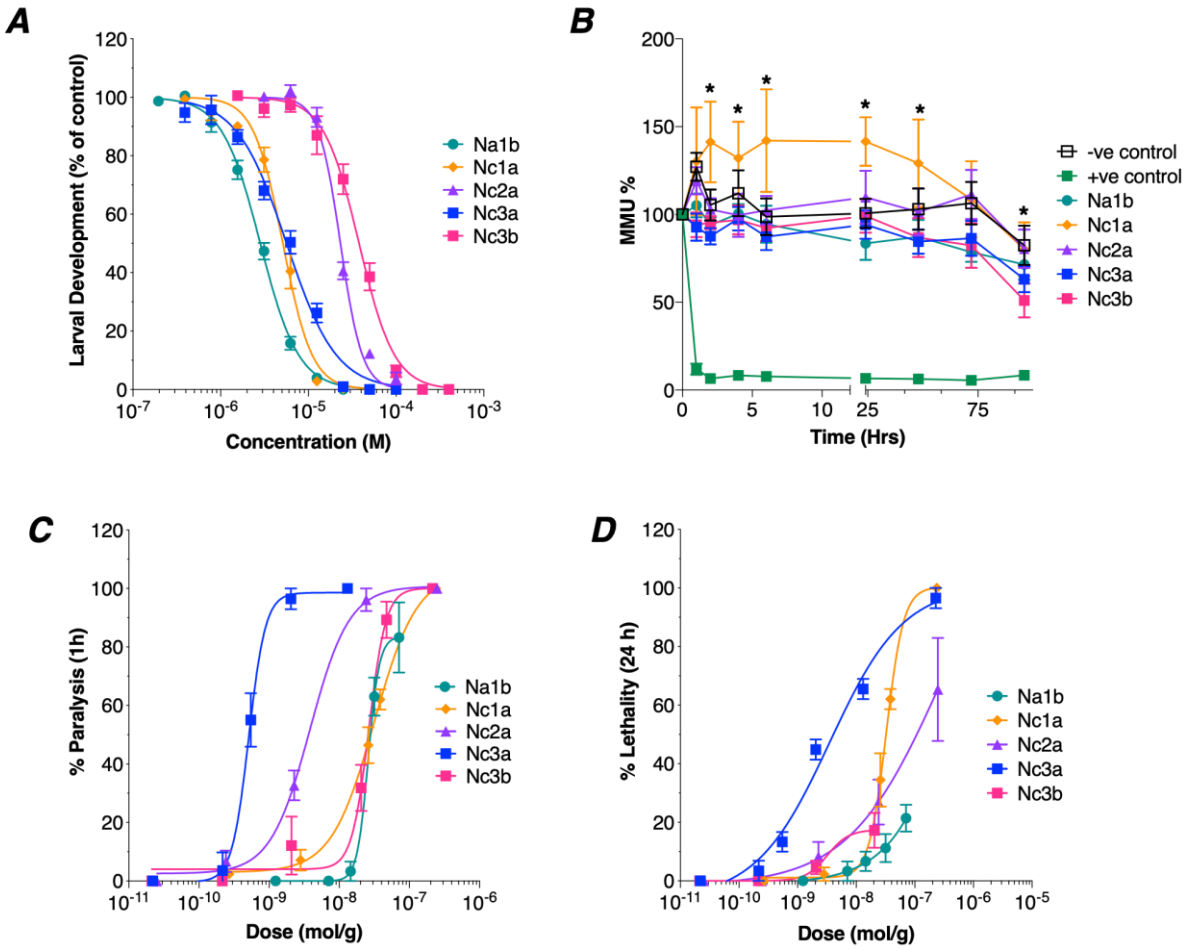
A
Larval Development (% of control)
Concentration (M)
Na1b
Nc1a
Nc2a
Nc3a
Nc3b
B
MMU %
Time (Hrs)
-ve control
+ve control
Na1b
Nc1a
Nc2a
Nc3a
Nc3b
C
% Paralysis (1h)
Dose (mol/g)
Na1b
Nc1a
Nc2a
Nc3a
Nc3b
D
% Lethality (24 h)
Dose (mol/g)
Na1b
Nc1a
Nc2a
Nc3a
Nc3b

Figure 6.

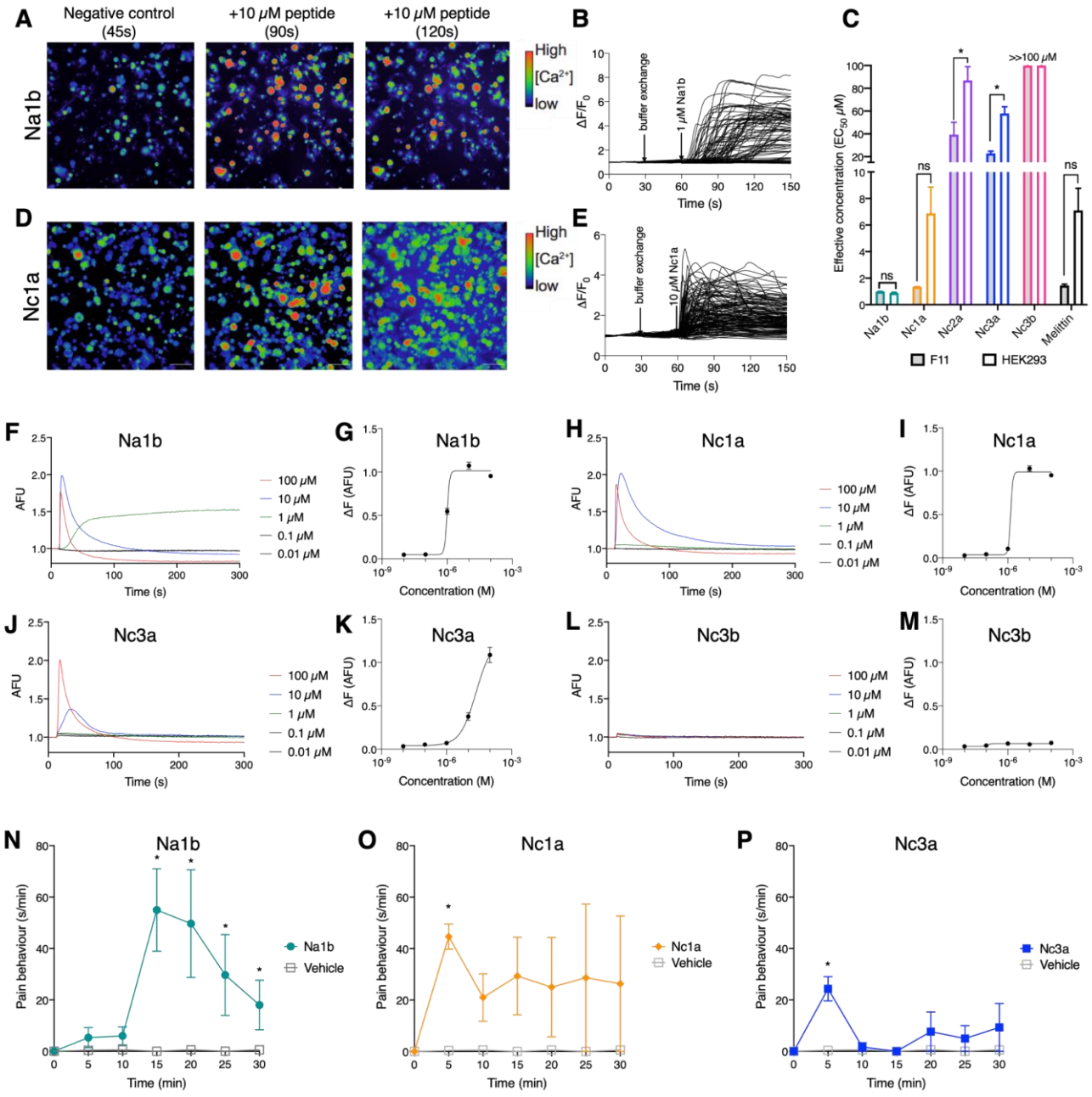
A
Negative control (45s)
+10 μM peptide (90s)
+10 μM peptide (120s)
Na1b
High [Ca2+] low
B
buffer exchange
1 μM Na1b
ΔF/F0
Time (s)
C
Effective concentration (EC50 μM)
>>100 μM
ns
Na1b
Nc1a
Nc2a
Nc3a
Nc3b
Melittin
F11
HEK293
D
Nc1a
E
buffer exchange
10 μM Nc1a
F
Na1b
AFU
100 μM
10 μM
1 μM
0.1 μM
0.01 μM
G
Na1b
ΔF (AFU)
Concentration (M)
H
Nc1a
I
Nc1a
J
Nc3a
K
Nc3a
L
Nc3b
M
Nc3b
N
Na1b
Pain behaviour (s/min)
Time (min)
Vehicle
O
Nc1a
P
Nc3a

Figure 7.

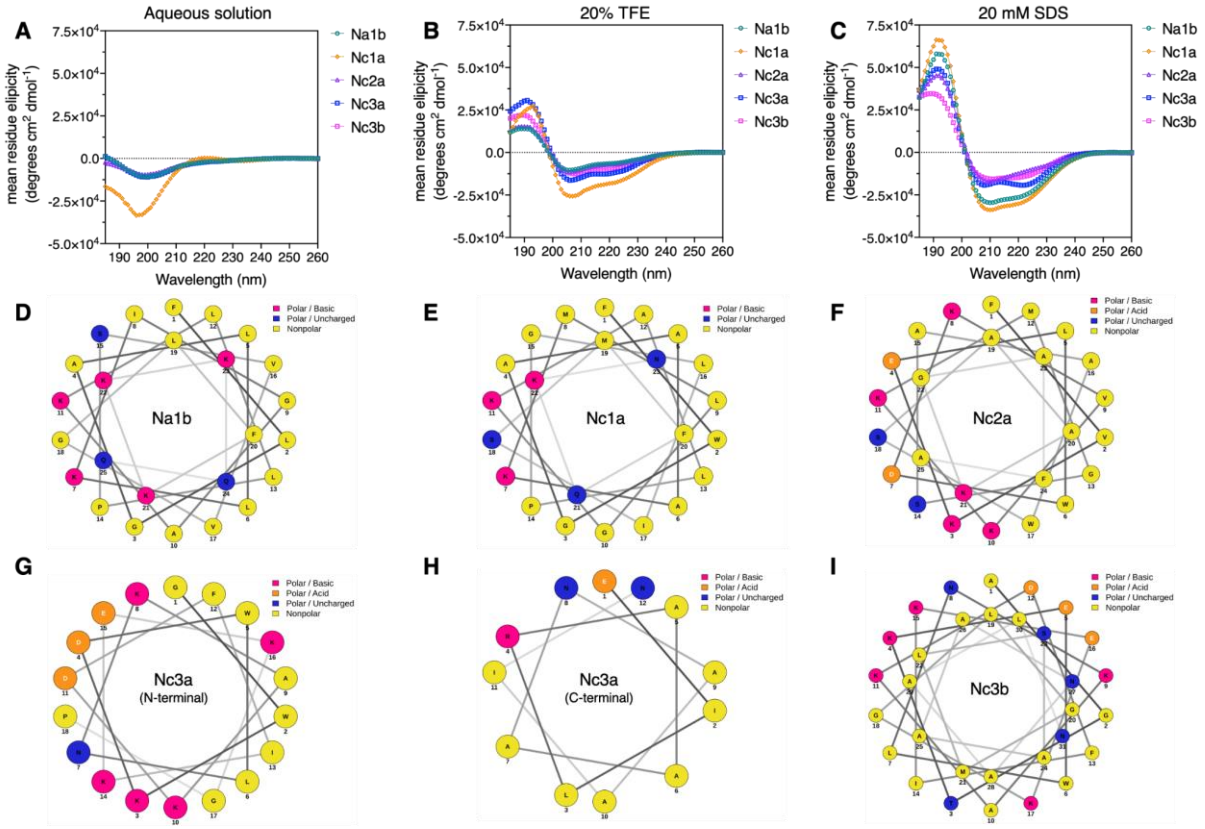
A
Aqueous solution
B
20% TFE
C
20 mM SDS
mean residue ellipicity (degrees cm^2 dmol^{-1})
Wavelength (nm)
Na1b
Nc1a
Nc2a
Nc3a
Nc3b
D
Na1b
E
Nc1a
F
Nc2a
G
Nc3a (N-terminal)
H
Nc3a (C-terminal)
I
Nc3b
Polar / Basic
Polar / Acid
Polar / Uncharged
Nonpolar

Figure 8.

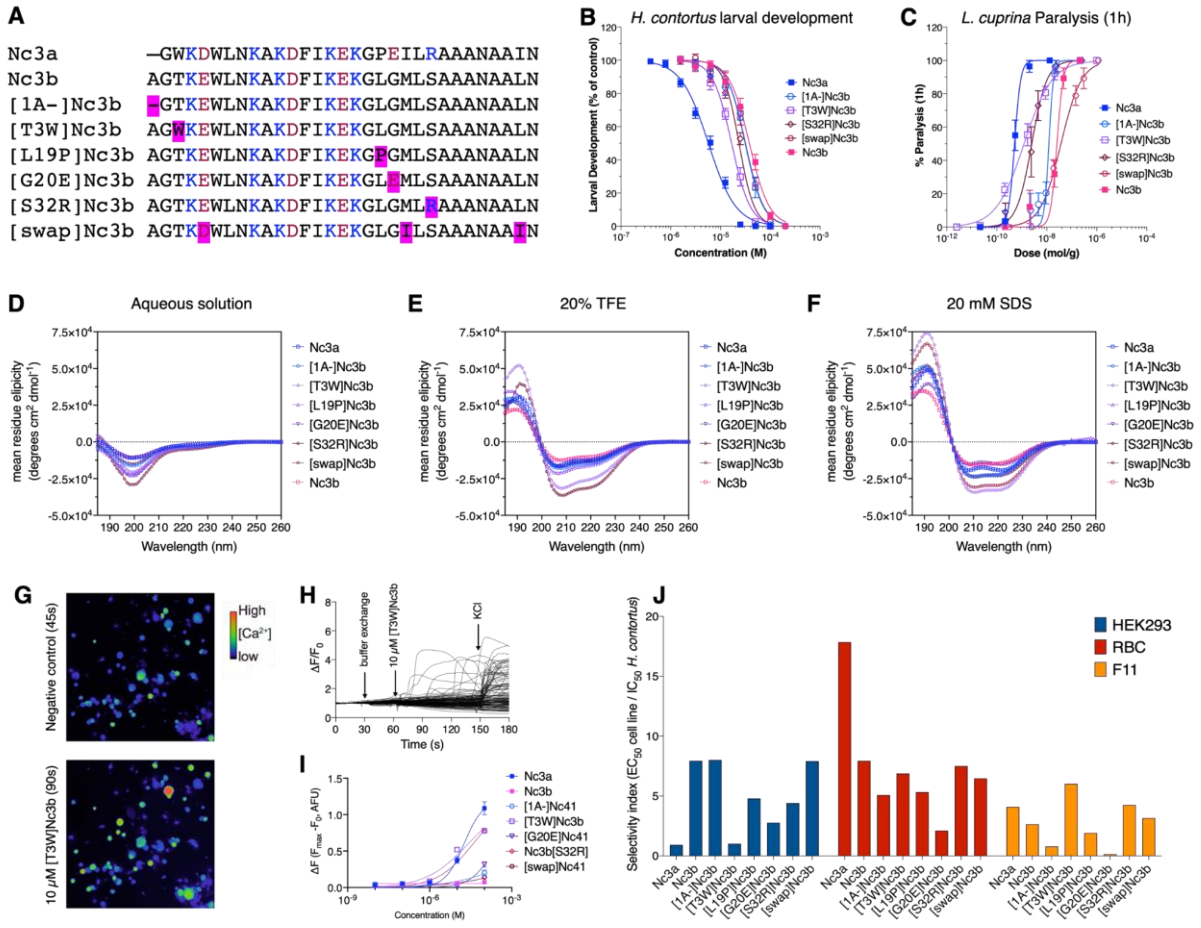
A
Nc3a —GWKDWLNKAKDFIKEKGPEILRAAANAAIN
Nc3b AGTKEWLNKAKDFIKEKGLGMLSAAANAALN
[1A-]Nc3b -GTKEWLNKAKDFIKEKGLGMLSAAANAALN
[T3W]Nc3b AGWKEWLNKAKDFIKEKGLGMLSAAANAALN
[L19P]Nc3b AGTKEWLNKAKDFIKEKGPGMLSAAANAALN
[G20E]Nc3b AGTKEWLNKAKDFIKEKGL-MLSAAANAALN
[S32R]Nc3b AGTKEWLNKAKDFIKEKGLGMLRAAANAALN
[swap]Nc3b AGTK-WLNKAKDFIKEKGLGILSAAANAATN
B
H. contortus larval development
Larval Development (% of control)
Concentration (M)
Nc3a
[1A-]Nc3b
[T3W]Nc3b
[S32R]Nc3b
[swap]Nc3b
Nc3b
C
L. cuprina Paralysis (1h)
% Paralysis (1h)
Dose (mol/g)
D
Aqueous solution
E
20% TFE
F
20 mM SDS
mean residue ellipicity (degrees cm2 dmol-1)
Wavelength (nm)
G
Negative control (45s)
10 μM [T3W]Nc3b (90s)
High
[Ca2+]
low
H
buffer exchange
10 μM [T3W]Nc3b
KCl
ΔF/F0
Time (s)
I
ΔF (Fmax-F0, AFU)
Concentration (M)
Nc3a
Nc3b
[1A-]Nc41
[T3W]Nc3b
[G20E]Nc41
Nc3b[S32R]
[swap]Nc41
J
Selectivity index (EC50 cell line / IC50 H. contortus)
HEK293
RBC
F11
Nc3a
Nc3b
[1A-]Nc3b
[T3W]Nc3b
[L19P]Nc3b
[G20E]Nc3b
[S32R]Nc3b
[swap]Nc3b

6 Tables

Table 1: Characteristics of anthelmintic ponericins isolated from *N. apicalis* and *N. commutata* venoms.

Ant	Toxin	Sequence	Monoisotopic mass (Da)		Net charge	Ponericin subfamily
			Theoretical	Observed		
N. apicalis	M-PONTX-Na1b	FLGALLKIGAKLLPSVVGLFKKKQQ	2695.7	2695.6	+5	W
N. commutata	M-PONTX-Nc1a	FWGAAAKMLGKALPGLISMFQKN	2478.3	2478.0	+3	W
	M-PONTX-Nc2a	FVKELWDKVKKMGSAAWSAAKGAFA	2725.4	2725.2	+3	L
	M-PONTX-Nc3a	GWKDWLNKAKDFIKEKGPEILRAAANAAIN	3366.8	3366.5	+2	G
	M-PONTX-Nc3b	AGTKEWLNKAKDFIKEKGLGMLSAAANAALN	3259.7	3259.5	+2	G

Table 2: Antimicrobial activity of ponericins. Minimum inhibitory concentrations (MIC, µM) of synthetic ponericins, colistin, and vancomycin against Gram-negative and Gram-positive bacterial pathogens from the genera *Escherichia*, *Klebsiella*, *Acinetobacter*, *Pseudomonas*, *Staphylococcus* and *Bacillus.* MIC values below 3 µM are shown in bold and shaded.

	Minimum inhibitory concentration (µM)						
	Na1b	Nc1a	Nc2a	Nc3a	Nc3b	Colistin	Vancomycin
E. coli ATCC 259922	5.9–11.8	25.8–51.6	11.7–46.9	**2.3–4.7**	>40	**0.02–0.11**	–
K. pneumoniae ATCC 13883	23.7–47.4	>40	>40	5.9–11.8	>40	**0.02–0.11**	–
A. baumannii ATCC 19606	**1.4–2.9**	12.91	23.7–47.4	**1.48**	>40	**0.11**	–
P. aeruginosa ATCC 27853	>40	>40	>40	11.8 – 23.7	>40	**0.22–0.43**	–
S. aureus ATCC 43300	**0.3–5.9**	**2.9–5.9**	>40	23.7–47.4	>40	–	**0.69–1.38**
B. subtilis ATCC 6051	**0.18–2.9**	**1.48–5.9**	5.9–11.8	**1.48–2.9**	>40	–	**0.17–0.35**

Table 3: Summary of bioassay data for synthetic ponericins. IC_{50}, concentrations that caused 50% inhibition of *H. contortus* larval development; PD_{50}, median paralytic dose, and LD_{50}, median lethal dose for insecticidal effects on *L. cuprina*; MIC, minimum concentration for inhibition of bacterial growth; CC_{50}, concentration required to induce 50% death of HEK293 cells; HC_{50}, concentrations required to lyse 50% of human red blood cells; EC_{50}, effective concentration for activation of F11 cells in a FLIPR assay. All errors are SEM. Active peptides are shaded.

Peptide	**Subfamily**	**Anthelmintic**	**Insecticidal (nmol g^{-1})**		**Antimicrobial**	**Cytotoxicity**	**Hemolysis**	**DRG**	**FLIPR (EC_{50} µM)**	
		(IC_{50} µM)	(PD_{50} 1h)	(LD_{50} 24h)	(lowest MIC, µM)	(CC_{50} µM)	(HC_{50} µM)	**assay**	F11	HEK293
Na1b	W	2.8 ± 0.3	25.8 ± 13.9	>100	0.18–2.9[a,b]	4.5–5.9	39.9–61.5	Strong	0.99 ± 0.01	0.89 ± 0.05
Nc1a	W	5.1 ± 0.9	31.4 ± 6.3	32.6 ± 11.3	1.48–5.9[a,b,c]	12.6–13.5	28.6–48.2	Strong	1.35 ± 0.01	6.88 ± 1.98
Nc2a	L	23.2 ± 8.9	38.1 ± 18.5	>100	5.9–11.8[b]	48.2–56.9	>250	Weak	39.4 ± 10.7	86.9 ± 12.1
Nc3a	G	5.6 ± 1.3	0.5 ± 0.03	3.5 ± 0.8	1.48–2.9[a,b]	5.2–6.8	>100	Strong	22.9 ± 1.95	57.9 ± 5.87
Nc3b	G	37.8 ± 7.4	26.4 ± 5.9	>100	>40	>300	>300	Inactive	>100	>100

[a] *Acinetobacter baumannii*
[b] *Bacillus subtilis*
[c] *Staphylococcus aureus*

Table 4: Summary of bioassay data for synthetic ponericin analogues. IC_{50}, concentrations that caused 50% inhibition of *H. contortus* larval development; PD_{50}, median paralytic dose, and LD_{50}, median lethal dose for insecticidal effects on *L. cuprina*; CC_{50}, concentration required to induce 50% death of HEK293 cells; HC_{50}, concentrations required to lyse 50% of human red blood cells; EC_{50}, effective concentration for activation of F11 cells in a FLIPR assay. All errors are SEM. Active peptides are shaded.

Peptide	**Anthelmintic**	**Insecticidal activity (nmol g^{-1})**		**Cytotoxicity**	**Hemolysis**	**DRG assay**	**FLIPR (EC_{50} µM)**	
	(IC_{50} µM)	(PD_{50} 1h)	(LD_{50} 24h)	(CC_{50} µM)	(HC_{50} µM)		F11	HEK293
Nc3a	5.6 ± 1.3	0.5 ± 0.03	3.5 ± 0.8	5.2–6.8	>100	Strong	22.9 ± 1.95	57.9 ± 5.87
[1A-]Nc3b	31.2 ± 3.9	12.1 ± 3.9	41.7 ± 18.3	>250	>150	Inactive	>100	>100
[T3W]Nc3b	16.6 ± 2.5	1.1 ± 0.9	12.1 ± 3.3	16.9	>100	Strong	24.5 ± 0.01	>100
[L19P]Nc3b	52.1 ± 11.8	>50	>50	>250	>250	Inactive	>100	>100
[G20E]Nc3b	>100	>50	>50	>250	>150	Inactive	>100	>100
[S32R]Nc3b	23.5 ± 8.3	2.5 ± 1.8	16.2 ± 4.8	>100	>150	Strong	12.1 ± 0.67	>100
[swap]Nc3b	31.6 ± 7.6	37.1 ± 4.9	>50	>250	>200	Inactive	>100	>100
Nc3b	37.8 ± 7.4	26.4 ± 5.9	32.1 ± 8.6	>300	>300	Inactive	>100	>100

1032